Celest Mech Dyn Astr (2013) 117:279–313
DOI 10.1007/s10569-013-9513-8

ORIGINAL ARTICLE

On optimal two-impulse Earth–Moon transfers in a four-body model

Francesco Topputo

Received: 18 October 2012 /Revised: 16 July 2013 Accepted: 6 August 2013 /
Published online: 30 August 2013

Abstract In this paper two-impulse Earth–Moon transfers are treated in the restricted four-body problem with the Sun, the Earth, and the Moon as primaries. The problem is formulated with mathematical means and solved through direct transcription and multiple shooting strategy. Thousands of solutions are found, which make it possible to frame known cases as special points of a more general picture. Families of solutions are defined and characterized, and their features are discussed. The methodology described in this paper is useful to perform trade-off analyses, where many solutions have to be produced and assessed.

Keywords Earth–Moon transfer · Low-energy transfer · Ballistic capture · Trajectory optimization · Restricted three-body problem · Restricted four-body problem

1 Introduction

The search for trajectories to transfer a spacecraft from the Earth to the Moon has been the subject of countless works. The Hohmann transfer represents the easiest way to perform an Earth–Moon transfer. This requires placing the spacecraft on an ellipse having the perigee on the Earth parking orbit and the apogee on the Moon orbit. By properly switching the gravitational attractions along the orbit, the spacecraft's motion is governed by only the Earth for most of the transfer, and by only the Moon in the final part. More generally, the patched-conics approximation relies on a Keplerian decomposition of the Solar System dynamics (Battin 1987). Although from a practical point of view it is desirable to deal with analytical solutions, the two-body problem being integrable, the patched-conics approximation inherently involves hyperbolic approaches upon arrival. This in turn asks for considerable costs (i.e. Δv maneuvers) to inject the spacecraft into the final orbit about the Moon.

Electronic supplementary material The online version of this article (doi:10.1007/s10569-013-9513-8) contains supplementary material, which is available to authorized users.

F. Topputo (✉)
Department of Aerospace Science and Technology, Politecnico di Milano,
Via La Masa, 34, 20156 Milan, Italy
e-mail: francesco.topputo@polimi.it

Low energy transfers have been found in the attempt to reduce the total cost for Earth–Moon transfers. They exploit the concept of temporary ballistic capture, or weak capture, which is defined in the framework of n-body problems (Belbruno 2004). It has been demonstrated that low-energy transfers may lower the arrival Δv, so entailing savings on the transfer cost (Belbruno and Miller 1993; Topputo et al. 2005b). A low energy transfer was used in the rescue of the *Hiten* mission (Belbruno and Miller 1993; Belbruno 2004), and, more recently, a similar transfer has been executed in the mission *GRAIL* (Hoffman 2009; Roncoli and Fujii 2010; Chung et al. 2010; Hatch et al. 2010). Low energy transfers are being preferred to standard patched-conics transfers for their appealing features, such as the lower cost, the extended launch windows, and the property of allowing for a fixed arrival epoch for any launch date within the launch window (Biesbroek and Janin 2000; Chung et al. 2010; Parker et al. 2011; Parker and Anderson 2011). The extended transfer time also benefits operations, check-outs, and out-gassing.[1] It has been demonstrated that the cost for low energy transfers can be further reduced by using low-thrust propulsion (Belbruno 1987; Mingotti et al. 2009a, 2012). The mission *SMART-1* performed such a combination successfully (Schoenmaekers et al. 2001). The low energy approach has also been extended to the case of interplanetary transfers (Topputo et al. 2005b; Hyeraci and Topputo 2010, 2013).

1.1 Low energy exterior and interior transfers

Low energy transfers can be classified into exterior and interior, according to the trajectory geometry. In the exterior transfers the spacecraft is injected into an orbit having the apogee at approximately four Earth–Moon distances. In this region, a small maneuver, combined with the perturbation of the Sun, makes it possible to approach the Moon from the exterior, and to perform a lunar ballistic capture (Belbruno and Miller 1993). It has been shown that the performances of the transfer can be improved by avoiding the mid-course maneuver (Belbruno and Carrico 2000) and by introducing a lunar gravity assist at departure (Mingotti et al. 2012). The exterior transfers exploit the gravity gradient of the Sun in a favorable way (Yamakawa et al. 1992, 1993). It has been found that these transfers can take place when the orbit is properly oriented with respect to the Sun, the Earth, and the Moon. More specifically, in a reference frame centered at the Earth, with the x-axis aligned with the Sun–Earth line, and with x growing in the anti-Sun direction, the exterior transfers can take place when the apogee lies either in the *second* or in the *fourth* quadrant (Belló-Mora et al. 2000; Circi and Teofilatto 2001; Ivashkin 2002; Circi and Teofilatto 2006).

Exterior transfers can be also viewed in the perspective of Lagrangian points dynamics (Belbruno 1994; Koon et al. 2000). In the coupled restricted three-body problem approximation, the four-body problem that governs the dynamics of the exterior transfers, is split into two restricted three-body problems having Sun, Earth and Earth, Moon as primaries, respectively. It can be shown that the first portion of the exterior transfer is close to the stable/unstable manifolds of the periodic orbits about either L_1 or L_2 of the Sun–Earth problem. Analogously, the second part (i.e. the lunar ballistic capture) is an orbit defined inside the stable manifold of the periodic orbits about L_2 in the Earth–Moon problem (Gómez et al. 2001; Koon et al. 2001; Parker 2006; Parker and Lo 2006). With this approach, second and fourth quadrant transfers are obtained by exploiting the dynamics of the Sun–Earth L_1 and L_2, respectively.

In the interior transfers most of the trajectory is defined within the Moon orbit. These transfers exploit the dynamics of the cislunar region in the Earth–Moon system (Conley

[1] http://moon.mit.edu/design.html, retrieved on 13 February 2012.

1968; Belbruno 1987; Miele and Mancuso 2001). As the equilibrium point is approached asymptotically (to keep the energy of the transfer low), interior transfers usually have long durations (Bolt and Meiss 1995; Schroer and Ott 1997; Macau 2000; Ross 2003). Also, multiple maneuvers are required to raise the orbit starting from low-altitude Earth parking orbits (Pernicka et al. 1995; Topputo et al. 2005a). Although for such long transfers perturbations may in principle produce significant effects, the solar perturbation is not crucial here, and interior transfers may be defined in the Earth–Moon restricted three-body problem. By postulating that the spacecraft would transit from the Earth region to the Moon region at the energy associated to that of L_1, it is possible to quantify the minimum cost for a transfer between two given orbits (Sweetser 1991). Other kinds of interior transfers exploit the resonances between the transfer orbit and the Moon. These require shorter flight times, though their energy level is greater than that of L_1 (Yagasaki 2004a,b; Mengali and Quarta 2005).

1.2 Statement of the problem

In this paper, two-impulse Earth–Moon transfers are studied. These are defined as follows. The spacecraft is initially in a low-altitude Earth parking orbit. A first impulse, assumed parallel to the velocity of the parking orbit, places the spacecraft on the transfer orbit. At the end of the transfer, a second impulse inserts the spacecraft into a low-altitude Moon orbit. This second impulse is again parallel to the velocity of the Moon parking orbit. Thus, the transfer is accomplished in a totally ballistic fashion; i.e. neither mid-course maneuvers nor other means of propulsion are considered during the cruise. A two-impulse transfer strategy involves maneuvering in the proximity of the Earth and Moon. Maneuvering in the direction of the local velocity maximizes the variations of spacecraft energy (Pernicka et al. 1995). Moreover, a mission profile including a low-Earth orbit is consistent with major architecture requirements (e.g., use of small/medium size launchers, in-orbit assembly of large structures, etc. Perozzi and Di Salvo 2008).

For the sake of a better comprehension of the results presented in this work, the departure and arrival orbits are chosen consistently with the existing literature. A 167 km circular Earth parking orbit, as well as a 100 km circular orbit about the Moon have been extensively used to compute Earth–Moon transfers (see Sect. 1.3). Thus, although the results presented in this paper can be easily extended to other orbits, for which no qualitative difference is expected, quantitatively, the two-impulse Earth–Moon transfers treated in this paper refer to

- an initial circular Earth orbit of altitude $h_i = 167\,\text{km}$;
- a final circular Moon orbit of altitude $h_f = 100\,\text{km}$.

1.3 Summary of previous contributions

A number of authors have dealt with Earth–Moon transfers between the two orbits defined above (Sweetser 1991; Yamakawa et al. 1992, 1993; Belbruno and Miller 1993; Pernicka et al. 1995; Yagasaki 2004a,b; Topputo et al. 2005a; Mengali and Quarta 2005; Assadian and Pourtakdoust 2010; Peng et al. 2010; Mingotti et al. 2012; Da Silva Fernandes and Marinho 2011). Table 1 represents an attempt of harmonization of all the solutions known to the author. For each solution, the cost (Δv) and the time-of-flight (Δt) are reported.[2] The two values are given with accuracy of m/s and day, respectively. As different dynamical mod-

[2] The patched-conics solutions (Hohmann, bielliptic, and biparabolic) have been calculated by assuming the gravitational parameters of the Earth and Moon equal to $3.986 \times 10^5\,\text{km}^3\text{s}^{-2}$ and $4.902 \times 10^3\,\text{km}^3\text{s}^{-2}$, respectively.

Table 1 Known examples of Earth–Moon transfers between a $h_i = 167$ km circular orbit about the Earth and a $h_f = 100$ km circular orbit about the Moon

References	Δv (m/s)	Δt (days)	Model	Type
Biparabolic	3947	∞	Patched two-body, 3D	E
Hohmann	3954	5		I
Biellipticˆ(†)	4221	90		E
Sweetser (1991)	3726	–	Restricted three-body, 2D	I
Yamakawa et al. (1992)ˆ(*),(‡)	3806	93	Bicircular restricted four-body, 2D	E
	3783	160		E+LGA
	3749	111		E+LGA
	3741	180		E+LGA
Belbruno and Miller (1993)	3838	160	Full ephemeris n-body, 3D	E+MGA
Yamakawa et al. (1993)ˆ(*),(‡)	3761	83	Restricted four-body, 2D	E+LGA
	3776	95		E+LGA
	3797	134		E+LGA
	3896	337		E+LGA
Pernicka et al. (1995)	3824	292	Restricted three-body, 2D	I
Yagasaki (2004a)ˆ(○)	3916	32	Restricted three-body, 2D	E
	3924	31		I
	3947	14		I
	3951	4		I
Yagasaki (2004b)ˆ(○)	3855	43	Bicircular restricted four-body, 2D	E+LGA
	3901	32		E
	3911	36		E+LGA
	3942	24		I
Topputo et al. (2005a)	3894	255	Restricted three-body, 2D	I
	3899	193		I
Mengali and Quarta (2005)	3861	85	Restricted three-body, 2D	I
	3920	68		I
	3950	14		I
	4005	3		I
Assadian and Pourtakdoust (2010)	3865	111	Restricted four-body, 3D	E
	3880	96		E
	4080	59		E
Peng et al. (2010)ˆ(*)	3908	112	Patched restricted three-body, 2D	E
	3908	121		E
	3915	113		E
	3920	108		E
Mingotti and Topputo (2011)	3793	88	Bicircularrestricted four-body, 2D	E+LGA
	3828	51		E
	3896	31		I
	3936	14		I
Da Silva Fernandes and Marinho (2011)	3857	87	Bicircular restricted four-body, 2D	E
	3866	86		E
	3901	32		I
	3944	14		I

References are ordered by year of publication. The cost (Δv) is either the sum of the two maneuvers (for two-impulse transfers) or the sum of all required maneuvers (for multi-impulse transfers); Δt is the time-of-flight. When more than four solutions are published (this is the case of Yamakawa et al. (1992); Yagasaki (2004a,b); Mengali and Quarta (2005); Mingotti and Topputo (2011); Da Silva Fernandes and Marinho (2011)), the four most representative results in terms of (Δv, Δt) are reported. The fourth column indicates the model in which these solutions are obtained. The fifth column specifies the type of transfer according to the geometry of the trajectory (I: Interior; E: Exterior; LGA: Lunar Gravity Assist)

ˆ(†) Apogee radius of 1.5×10^6 km; ˆ(*) $h_i = 200$ km; ˆ(‡) Δv of 573 and 676 m/s added to the results published in Yamakawa et al. (1992) and Yamakawa et al. (1993), respectively, to achieve a 100 km circular orbit around the Moon; ˆ(○) speed unit of 1024.5 m/s and time unit of 4.341 days used to extract data from scaled values available

els can be used to compute Earth–Moon transfers, the reported solutions have to be framed into the model they are achieved with; this is also reported in Table 1. The solutions are labeled in terms of transfer type (interior or exterior), as discussed in Sect. 1.1; the presence of lunar gravity assists (LGA) is also indicated. The reader can refer to the works cited in Table 1 for details.

1.4 Motivations

Figure 1 reports the solutions of Table 1 in the $(\Delta t, \Delta v)$ plane. Each solution taken from the literature corresponds to a point in this plane. As expected, the cost of transfers tends to reduce for increasing transfer time. Moreover, it can be noted that the solutions of different studies tend to cluster together. It is conjectured that these points represent just traces of a more intricate structure, which characterizes the $(\Delta t, \Delta v)$ space of solutions of Earth–Moon transfers. Thus, questions arise. Is it possible *to reduce* known examples to special points of a more general picture? What does the solution structure of two-impulse Earth–Moon transfers look like in the $(\Delta t, \Delta v)$ plane? No matter if the transfers are interior or exterior; being different solutions of the *same* problem, they have to be thought of as special branches of a *common* picture, which may even contain unknown results.

1.5 Assumptions and scopes

The aim of this work is to characterize the two-impulse Earth–Moon transfers between two given orbits within a restricted four-body model. In doing so, the same nonlinear boundary value problem as in Yagasaki (2004b) is numerically solved to obtain the results. A number of transfer families are found, including many optimal ones previously reported. The focus is to reveal the structure underlying the points in Fig. 1. Thus, patched-conics, interior, and exterior transfers have to be obtained in a common dynamical framework. This means that the dynamical model should suffice to allow the reproduction of all these solutions. As patched-conics, interior, and exterior transfers are defined in the two-, three-, and four-body problems, respectively, a four-body model is to be used. On the other hand, the model has to be sufficiently simple to allow the derivation of a general solutions set, without introducing specific mission parameters (e.g., launch dates, angular parameters on departure and arrival orbits, etc). With reference to Table 1, the *planar bicircular restricted four-body problem* is chosen. This model is deemed appropriate to catch the basic dynamics characterizing the Sun–Earth–Moon problem (Simó et al. 1995; Yamakawa et al. 1992; Yagasaki 2004b; Mingotti et al. 2012; Mingotti and Topputo 2011; Da Silva Fernandes and Marinho 2011).

Another parameter to set is the maximum transfer duration. This has to be limited to avoid the indefinite growing of solutions. In literature, solutions with a time-of-flight of up to 300 days exist (see Table 1; Fig. 1), and Earth–Moon transfers requiring as much as 2 years have been found (Bolt and Meiss 1995). However, in this work, a lunar transfer requiring hundreds of days is not deemed a viable option for real missions. For this reason, the characterization of two-impulse Earth–Moon transfers is restricted to those solutions whose duration is less than 100 days (i.e. the search is limited to the white area in Fig. 1). Although this could appear too restrictive, it will be shown that the selected search space possesses a sufficiently rich structure, which may contain novel transfer families. In this search space, the front of Pareto-efficient solutions is reconstructed. (These are the solutions showing the best balance between cost and transfer time; see Definition 2.) The aim is to build a catalogue from which preliminary estimates on the transfer cost could be extracted if the transfer time was specified (or vice-versa).

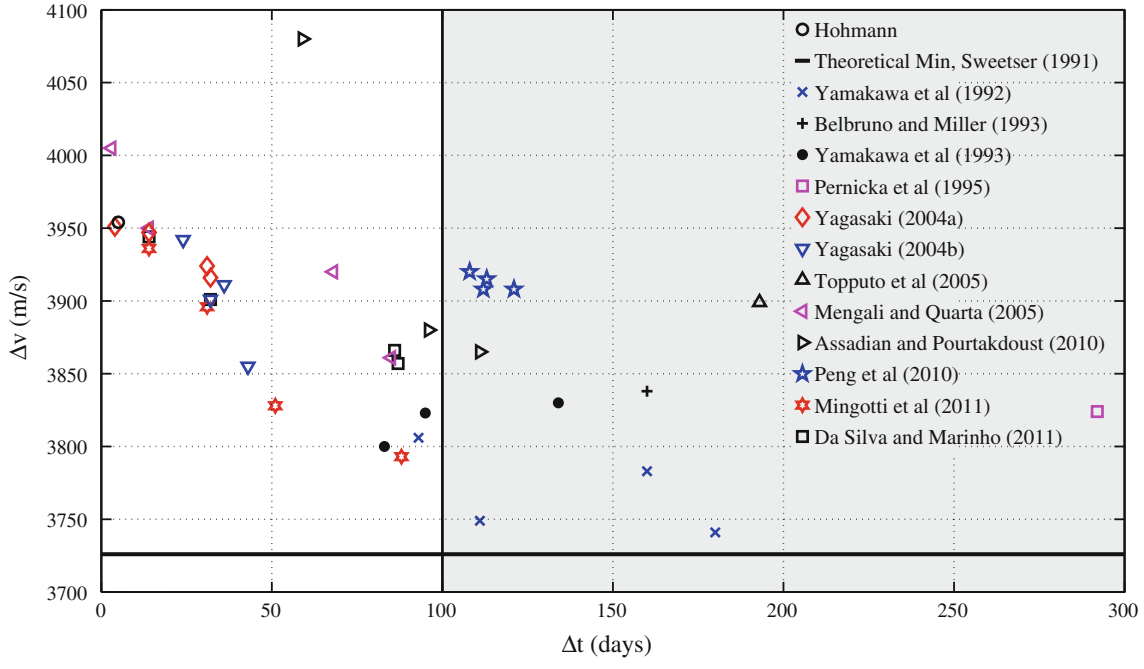

Fig. 1 Solutions of Table 1 reported on the $(\Delta t, \Delta v)$ plane. The *horizontal line* represents the theoretical minimum (Sweetser 1991); the *vertical line* separates the region investigated in this paper (*white*) from the rest of the solutions space

Summarizing, the scopes of the paper are:

1. to optimize two-impulse Earth–Moon transfers in the planar bicircular restricted four-body problem;
2. to reconstruct the solution space in the $(\Delta t, \Delta v)$ plane, $\Delta t \leq 100$ days, and to extract the set of Pareto-efficient solutions;
3. to characterize the solution structure by identifying families of transfer orbits, some of which may be unknown in literature.

The remainder of the paper is structured as follows. In Sect. 2 the background notions are recalled (restricted three-/four-body problem and temporary ballistic capture). In Sect. 3 the optimization problem is treated in terms of first guess solutions, optimization algorithms, and implementation issues. In Sect. 4 the optimized solutions are presented and discussed on a global basis. Specific results are characterized and families of solutions are defined in Sect. 5. Concluding, final considerations are given in Sect. 6.

2 Background

2.1 Planar circular restricted three-body model

In the Planar Circular Restricted Three-Body Problem (PCRTBP) two primary bodies P_1, P_2 of masses $m_1 > m_2 > 0$, respectively, move under mutual gravity on circular orbits about their common center of mass. The third body, P, assumed of infinitesimal mass, moves under the gravity of the primaries, and in the same plane. The motion of the primaries is not affected by P. In the present case, P represents a spacecraft, and P_1, P_2 represent the Earth and the Moon, respectively. Let $\mu = m_2/(m_1 + m_2)$ denote the mass ratio of P_2 to the total mass.

The motion of P relative to a co-rotating coordinate system (x, y) with the origin at the center of mass of the two bodies, and in normalized distance, mass, and time units, is described by (Szebehely 1967)

$$\ddot{x} - 2\dot{y} = \frac{\partial \Omega_3}{\partial x}, \qquad \ddot{y} + 2\dot{x} = \frac{\partial \Omega_3}{\partial y}, \tag{1}$$

where the effective potential, Ω_3, is given by

$$\Omega_3(x, y) = \frac{1}{2}(x^2 + y^2) + \frac{1-\mu}{r_1} + \frac{\mu}{r_2} + \frac{1}{2}\mu(1-\mu), \tag{2}$$

with $r_1 = [(x+\mu)^2 + y^2]^{1/2}, r_2 = [(x+\mu-1)^2 + y^2]^{1/2}$ as P_1, P_2 are located at $(-\mu, 0), (1-\mu, 0)$, respectively.

The motion described by Eqs. (1) has five equilibrium points $L_k, k = 1, \ldots, 5$, known as the Euler–Lagrange libration points. Three of these, L_1, L_2, L_3, lie along the x-axis;, the other two points, L_4, L_5, lie at the vertices of two equilateral triangles with common base extending from P_1 to P_2. The system of differential equations (1) admits an integral of motion, the Jacobi integral,

$$J(x, y, \dot{x}, \dot{y}) = 2\Omega_3(x, y) - (\dot{x}^2 + \dot{y}^2). \tag{3}$$

The values of the Jacobi integral at the points $L_i, C_i = J(L_i), i = 1, \ldots, 5$, satisfy $C_1 > C_2 > C_3 > C_4 = C_5 = 3$. Table 2 reports the collinear libration points location and their Jacobi energy for the Earth–Moon system.

Table 2 Location of the collinear Lagrange points, x_{L_i}, and their Jacobi energy, C_i, $i = 1, 2, 3$, for $\mu = 0.0121506683$

	x_{L_i}	C_i
L_1	0.8369147188	3.2003449098
L_2	1.1556824834	3.1841641431
L_3	−1.0050626802	3.0241502628

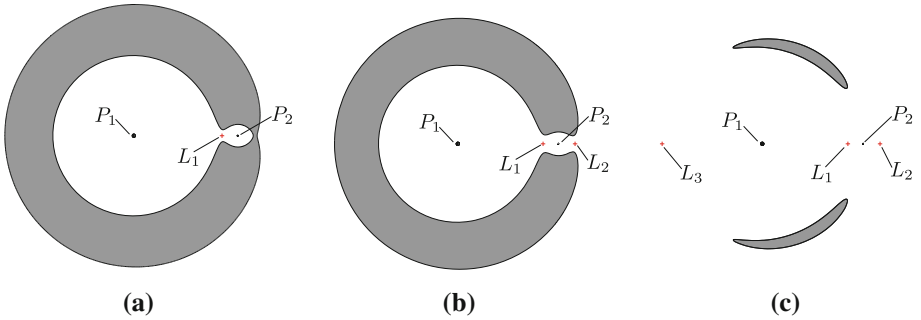

Fig. 2 Hill's regions (*white*) and forbidden regions (*grey*) for varying energies. **a** $C_2 \leq J < C_1$; **b** $C_3 \leq J < C_2$; **c** $C_{4,5} \leq J < C_3$

The projection of the energy manifold

$$\mathcal{J}(C) = \{(x, y, \dot{x}, \dot{y}) \in \mathbb{R}^4 | J(x, y, \dot{x}, \dot{y}) = C\}, \tag{4}$$

onto the configuration space (x, y) is called Hill's region. In the PCRTBP, the motion of P is always confined to the Hill regions of the corresponding Jacobi energy C. The boundary of Hill's region is a zero-velocity curve. Hill's regions vary with the Jacobi energy C (see Fig. 2). In this model, for P to transfer from P_1 to P_2 (and vice versa), the condition $J < C_1$ has to be respected. In particular, this can occur at four different energy ranges: a) $C_2 \leq J < C_1$; b) $C_3 \leq J < C_2$; c) $C_{4,5} \leq J < C_3$; d) $J < C_{4,5}$. In case a), P can transit through the small allowed region about L_1, and therefore interior transfers only are admitted (Fig. 2a). In case b), P_2 may be reached from either L_1 or L_2, and thus both interior and exterior transfers are allowed (Fig. 2b). In cases c), P can approach P_2 from any direction (Fig. 2c). In case d) P is allowed to move in the whole physical space. As the mechanical energy of P increases in moving from case a) to d), the cost of the transfers increase accordingly.

2.2 Planar bicircular restricted four-body model

The Planar Bicircular Restricted Four-Body Problem (PBRFBP) incorporates the perturbation of a third primary, P_3, the Sun in our case, into the PCRTBP described above. P_3 is assumed to revolve in a circular orbit around the center of mass of P_1–P_2. This model is not coherent as all the primaries are assumed to move in circular orbits. Nevertheless, it catches basic insights of the real four-body dynamics (Castelli 2011); this holds as the eccentricities of the Earth and Moon orbits are 0.0167 and 0.0549, respectively, and the Moon orbit inclination on the ecliptic is 5°.

Table 3 Physical constants used in this work (taken from Simó et al. (1995))

Symbol	Value	Units	Meaning
μ	$1.21506683 \times 10^{-2}$	–	Earth–Moon mass parameter
m_s	3.28900541×10^{5}	–	Scaled mass of the Sun
ρ	3.88811143×10^{2}	–	Scaled Sun–(Earth + Moon) distance
ω_s	$-9.25195985 \times 10^{-1}$	–	Scaled angular velocity of the Sun
l_{em}	3.84405000×10^{8}	m	Earth–Moon distance
ω_{em}	$2.66186135 \times 10^{-6}$	s^{-1}	Earth–Moon angular velocity
R_e	6378	km	Mean Earth's radius
R_m	1738	km	Mean Moon's radius
h_i	167	km	Altitude of departure orbit
h_f	100	km	Altitude of arrival orbit
DU	3.84405000×10^{8}	m	Distance unit
TU	4.34811305	days	Time unit
VU	1.02323281×10^{3}	$m\,s^{-1}$	Speed unit

The constants used to describe the Sun perturbation (m_s, ρ, ω_s) meet the length, time, and mass normalization of the PCRTBP. The units of distance, time, and speed are used to map scaled quantities into physical units

The equations of motion of the PBRFBP are (Simó et al. 1995; Yagasaki 2004b)

$$\ddot{x} - 2\dot{y} = \frac{\partial \Omega_4}{\partial x}, \qquad \ddot{y} + 2\dot{x} = \frac{\partial \Omega_4}{\partial y}, \tag{5}$$

where the four-body effective potential, Ω_4, reads

$$\Omega_4(x, y, t) = \Omega_3(x, y) + \frac{m_s}{r_3(t)} - \frac{m_s}{\rho^2}(x\cos(\omega_s t) + y\sin(\omega_s t)). \tag{6}$$

In Eq. (6) t is the time, m_s is the mass of the Sun, ρ is the distance between the Sun and the Earth–Moon barycenter, and ω_s is the angular velocity of the Sun in the Earth–Moon rotating frame; the phase angle of the Sun is $\theta(t) = \omega_s t$. Thus, the present location of the Sun is $(\rho\cos(\omega_s t), \rho\sin(\omega_s t))$, and therefore the Sun-spacecraft distance is

$$r_3(t) = \left[(x - \rho\cos(\omega_s t))^2 + (y - \rho\sin(\omega_s t))^2\right]^{1/2}. \tag{7}$$

It is worth pointing out that the Sun *is not* at rest in the reference frame adopted in Eqs. (5). This causes the loss of autonomy, and makes the PBRFBP a time-dependent model (see Eqs. (6)–(7)). This is a great departure from the PCRTBP as both the equilibrium points and the Jacobi integral vanish. Table 3 reports the value of the physical constants used in this study and their associated units of distance, time, and speed according to the normalization of the PCRTBP.

2.3 Ballistic capture

For the analysis below it is convenient to define the ballistic capture of P by P_2; i.e. the ballistic capture of the spacecraft by the Moon. Let $\boldsymbol{x}(t)$ be a solution of Eqs. (5), $\boldsymbol{x}(t) = (x(t), y(t), \dot{x}(t), \dot{y}(t))$, and let $H_2(\boldsymbol{x})$ be the Kepler energy of P with respect to P_2,

$$H_2 = \frac{1}{2}v_2^2 - \frac{\mu}{r_2}, \tag{8}$$

where v_2 is the speed of P relative to a P_2-centered inertial reference frame,[3]

$$v_2 = \left[(\dot{x} - y)^2 + (\dot{y} + x + \mu - 1)^2\right]^{1/2}. \tag{9}$$

Definition 1 (Ballistic captures) P is ballistically captured by P_2 at time t_1 if $H_2(\boldsymbol{x}(t_1)) \leq 0$. It is temporary ballistically captured by P_2 for finite times $t_1, t_2, t_1 < t_2$, if it is ballistically captured at any time $t \in [t_1, t_2]$ and $H_2(\boldsymbol{x}(t)) > 0$ for $t < t_1$ and $t > t_2$. It is permanently captured by P_2 if it is ballistically captured for all times $t \geq t_3$, for a finite time t_3.

These are the standard definitions of ballistic captures (see Belbruno (2004)). In the frame of Earth–Moon transfers, P can experience temporary ballistic captures only. For the capture to be permanent, a dissipative force must act upon P (Winter et al. (2003); De Melo and Winter 2006). To assess if Earth–Moon transfers exhibit temporary ballistic capture upon Moon arrival it is sufficient to check the sign of the right-hand side of Eq. (8) at the final time. (See Belbruno (2004); Belbruno et al. (2008); Topputo et al. (2008); Topputo and Belbruno (2009); Belbruno et al. (2010); Circi (2012) for more details on ballistic capture).

The angular momentum is another two-body indicator that can be used to understand the motion upon Moon arrival. As the motion is planar, the angular momentum $\boldsymbol{h}_2$ of P with respect to P_2 is perpendicular to the plane (x, y), and its magnitude is given by

$$h_2 = (x + \mu - 1)(\dot{y} + x + \mu - 1) - y(\dot{x} - y). \tag{10}$$

At arrival, direct or retrograde orbits with respect to the Moon can be detected by simply checking the sign of the right-hand side of Eq. (10) at the final time.

3 Optimization of two-impulse Earth–Moon transfers

Two impulse transfers are defined as follows. The spacecraft is assumed to be in a circular orbit about the Earth of scaled radius $r_i = (R_e + h_i)/DU$. At the initial time, t_i, an impulse of magnitude Δv_i injects the spacecraft into a transfer trajectory; Δv_i is aligned with the local circular velocity whose magnitude is $\sqrt{(1-\mu)/r_i}$. At the final time, t_f, an impulse of magnitude Δv_f inserts the spacecraft into the final orbit around the Moon. This orbit has scaled radius $r_f = (R_m + h_f)/DU$; Δv_f is aligned with the local circular velocity whose magnitude is $\sqrt{\mu/r_f}$. The total cost of the transfer is $\Delta v = \Delta v_i + \Delta v_f$ and the transfer time is $\Delta t = t_f - t_i$.

3.1 Definition of the optimization problem

Let $\boldsymbol{x}_i = (x_i, y_i, \dot{x}_i, \dot{y}_i)$ be the initial transfer state. This is at a physical distance r_i from the Earth, and has the velocity aligned with the local circular velocity if

$$(x_i + \mu)^2 + y_i^2 - r_i^2 = 0, \tag{11}$$

$$(x_i + \mu)(\dot{x}_i - y_i) + y_i(\dot{y}_i + x_i + \mu) = 0, \tag{12}$$

are both verified (Yagasaki 2004b). (The reader can refer to Eq. (34) in Appendix 1 for the transformation from the synodic to the Earth-centered, inertial frame.) For brevity, these two

[3] See Appendix 1 for the coordinate transformation behind (9) and (10).

initial conditions are indicated as $\boldsymbol{\psi}_i(\boldsymbol{x}_i) = \mathbf{0}$, where $\boldsymbol{\psi}_i$ is the two-dimensional vector valued function of $\boldsymbol{x}_i$ given by the left-hand sides of (11)–(12). Under these initial conditions, the cost for the initial maneuver is

$$\Delta v_i = \sqrt{(\dot{x}_i - y_i)^2 + (\dot{y}_i + x_i + \mu)^2} - \sqrt{\frac{1-\mu}{r_i}}, \tag{13}$$

which can be thought as a scalar, nonlinear function of $\boldsymbol{x}_i$; i.e. $\Delta v_i(\boldsymbol{x}_i)$.

Analogously, let $\boldsymbol{x}_f = (x_f, y_f, \dot{x}_f, \dot{y}_f)$ be the final transfer state. In order to arrive at a circular orbit of radius r_f around the Moon, with the velocity vector aligned with the local circular velocity, $\boldsymbol{x}_f$ must satisfy

$$(x_f + \mu - 1)^2 + y_f^2 - r_f^2 = 0, \tag{14}$$

$$(x_f + \mu - 1)(\dot{x}_f - y_f) + y_f(\dot{y}_f + x_f + \mu - 1) = 0. \tag{15}$$

Equations (14)–(15) are denoted as $\boldsymbol{\psi}_f(\boldsymbol{x}_f) = \mathbf{0}$; the two-dimensional vector valued function $\boldsymbol{\psi}_f$ is defined by the left-hand sides of (14)–(15). Under these final conditions, the arrival maneuver can be quantified by

$$\Delta v_f = \sqrt{(\dot{x}_f - y_f)^2 + (\dot{y}_f + x_f + \mu - 1)^2} - \sqrt{\frac{\mu}{r_f}}, \tag{16}$$

which is a scalar, nonlinear function of the final state; i.e. $\Delta v_f(\boldsymbol{x}_f)$. We can now proceed to state the optimization problem as follows.

Statement of the problem *Let $\boldsymbol{x}(t) = \varphi(\boldsymbol{x}_i, t_i; t)$ be a solution of (5), integrated from $(\boldsymbol{x}_i, t_i)$ to $t \geq t_i$. The optimization problem for two-impulse Earth–Moon transfers consists of finding $\{\boldsymbol{x}_i, t_i, t_f\}$, $t_f > t_i$, such that $\boldsymbol{\psi}_i(\boldsymbol{x}_i) = \mathbf{0}$, $\boldsymbol{\psi}_f(\boldsymbol{x}_f) = \mathbf{0}$, where $\boldsymbol{x}_f = \varphi(\boldsymbol{x}_i, t_i; t_f)$, and the function*

$$\Delta v(\boldsymbol{x}_i, t_i, t_f) = \Delta v_i(\boldsymbol{x}_i) + \Delta v_f(\varphi(\boldsymbol{x}_i, t_i; t_f)) \tag{17}$$

is minimized.

3.2 Forming an initial guess

From (17) it can be inferred that a two-impulse Earth–Moon transfer is uniquely specified once the *six* scalars $\{\boldsymbol{x}_i, t_i, t_f\}$ are given. In principle, one can guess the initial state, the initial time, and the final time, and check if the boundary conditions (11)–(12) and (14)–(15) are satisfied, and the objective function (17) is minimized. In the most likely event in which either the boundary conditions are violated or the objective function is not minimized, the guess can be used to define an initial solution, or first guess solution. This can be treated in an optimization framework, where both the boundary conditions and the minimization of the objective function are enforced.

Since this work aims at reconstructing the totality of solutions of two-impulse Earth–Moon transfers, thousands of initial guesses have to be processed to find locally optimal solutions. This can be done by performing a systematic search (i.e. a grid sampling) within the space in which the six scalars are defined. However, systematic searches suffer from the curse of dimensionality, and the high nonlinearities characterizing most Earth–Moon transfers would require a fine sampling of the variables. From this perspective, it would be desirable to guess as few numbers as possible. A transformation has been developed to define first guess solutions by specifying *four* scalars only. With reference to Fig. 3, these quantities are:

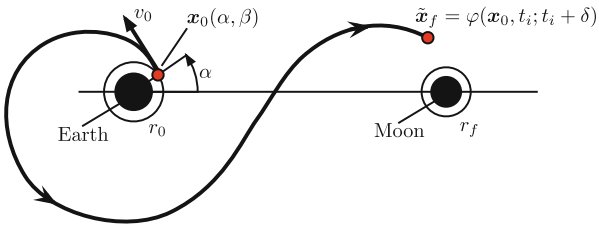

Fig. 3 Direct shooting of initial guess solutions

α, an angle defined on the Earth circular parking orbit;
β, the initial-to-circular velocity ratio;
t_i, the initial time;
δ, the transfer duration.

Given $\{\alpha, \beta, t_i, \delta\}$, the construction of initial guess solutions is straightforward. Let $r_0 = r_i$ and $v_0 = \beta\sqrt{(1-\mu)/r_0}$, the initial transfer state, $\boldsymbol{x}_0(\alpha, \beta) = (x_0, y_0, \dot{x}_0, \dot{y}_0)$, reads

$$x_0 = r_0\cos\alpha - \mu, \quad y_0 = r_0\sin\alpha, \quad \dot{x}_0 = -(v_0 - r_0)\sin\alpha, \quad \dot{y}_0 = (v_0 - r_0)\cos\alpha. \quad (18)$$

In Eq. (18), α determines the location of the initial point on the circular orbit, and β specifies the initial velocity, which is already aligned with the circular velocity. It is easy to verify that $\boldsymbol{x}_0(\alpha, \beta)$ automatically satisfies Eqs. (11)–(12); i.e. $\boldsymbol{\psi}_i(\boldsymbol{x}_0(\alpha, \beta)) = \boldsymbol{0}$, $\forall\{\alpha, \beta\}$.

The final state is defined by integrating $\boldsymbol{x}_0$ in the time span $[t_i,\ t_i+\delta]$; i.e. $\tilde{\boldsymbol{x}}_f(\alpha, \beta, t_i, \delta) = \varphi(\boldsymbol{x}_0(\alpha, \beta), t_i; t_i + \delta)$. If $\boldsymbol{\psi}_f(\tilde{\boldsymbol{x}}_f) = \boldsymbol{0}$ and $\Delta v(\boldsymbol{x}_0(\alpha, \beta), t_i, \delta)$ is minimum, then the combination $\{\alpha, \beta, t_i, \delta\}$ produces an optimal solution; otherwise, it defines an initial solution for a subsequent optimization step (see Fig. 3).

The search of first guess solutions can be further specialized by defining the set of admissible parameters. The selection of lower and upper bounds for each parameter sets the four-dimensional hypercube to sample (this is the reason why δ is the transfer duration and *not* the final time; (Armellin et al. 2010)). As for the first parameter, it is straightforward that $\alpha \in [0,\ 2\pi]$. The second parameter is allowed to be $\beta \in [1,\ \sqrt{2}]$, where $\beta = 1$ sets the circular velocity, while $\beta = \sqrt{2}$ defines the Earth-escape velocity. As for t_i, setting the initial time specifies the initial angular position of the Sun through $\theta_i = \omega_s t_i$ (see Eqs. (6)–(7)). Thus, $t_i \in [0,\ 2\pi/\omega_s]$ yields $\theta_i \in [0,\ 2\pi]$; i.e. any possible relative configuration of Sun, Earth, and Moon is considered. The transfer duration $\delta \in [0, T]$ is bounded by T, which is the maximum prescribed transfer time. First guess transfers with durations of up to 100 days are obtained by setting $T \cong 23\,TU$ (see Table 3).

Let $I_\alpha, J_\beta, K_{t_i}, L_\delta$ be the number of points in which the domains of $\alpha, \beta, t_i, \delta$ defined above are discretized, respectively. A direct shooting of first guess solutions is implemented through Algorithm 1. The generic first guess *orbit*, $\boldsymbol{\gamma}^{(ijkl)}$, can be used to initiate the subsequent trajectory optimization.

3.3 Solution by direct transcription and multiple shooting

Optimal two-impulse Earth–Moon transfers are found with a direct transcription and multiple shooting approach. Direct transcription maps a differential optimal control problem into an algebraic nonlinear programming (NLP) problem; see Enright and Conway (1992); Betts (1998) for details. This method has shown robustness and versatility when used to derive trajectories defined in highly nonlinear vector fields (Mingotti et al. 2009a,b, 2011a,b, 2012). Moreover, it does not require the explicit derivation of the necessary conditions of optimality, and it is less sensitive to variations of the first guess solution.

Algorithm 1 Pseudo code for first guess solution generation.

```
for i = 1 → I_α do
  α^(i) = 2π(i − 1)/(I_α − 1)
  for j = 1 → J_β do
    β^(j) = 1 + (√2 − 1)(j − 1)/(J_β − 1)
    for k = 1 → K_{t_i} do
      t_i^(k) = 2π/ω_s (k − 1)/(K_{t_i} − 1)
      for l = 1 → L_δ do
        δ^(l) = T(l − 1)/(L_δ − 1)
        γ^(ijkl) = {φ(x_0(α^(i), β^(j)), t_i^(k); t_i^(k) + δ), δ ≤ δ^(l)}
      end for
    end for
  end for
end for
```

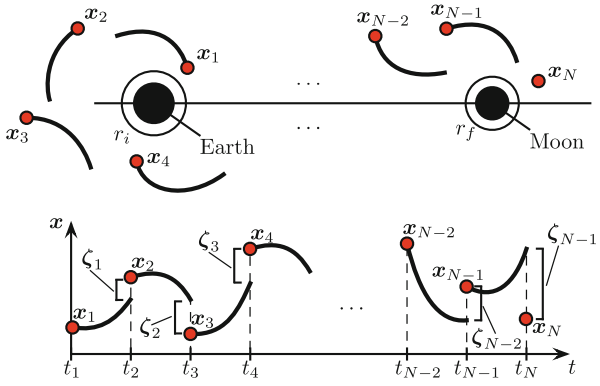

Fig. 4 Direct transcription and multiple shooting optimization scheme

Let the PBRFBP Eqs. (5) be written in the first-order form $\dot{\boldsymbol{x}} = \boldsymbol{f}(\boldsymbol{x}, t)$, and let $\boldsymbol{x}(t)$ be a solution. This is discretized over a uniform time grid, which is made up by N points such that $t_1 = t_i, t_N = t_f$, and

$$t_j = t_1 + \frac{j-1}{N-1}(t_N - t_1), \qquad j = 1, \ldots, N. \tag{19}$$

Let $\boldsymbol{x}_j = (x_j, y_j, \dot{x}_j, \dot{y}_j)$ be the solutions at the j-th mesh point; i.e. $\boldsymbol{x}_j = \boldsymbol{x}(t_j), j = 1, \ldots, N$. The multiple shooting method requires the dynamics (5) to be integrated within the $N-1$ intervals $[t_j,\ t_{j+1}]$ by taking $\boldsymbol{x}_j$ as initial condition (see Fig. 4). The continuity of position and velocity requires the defects

$$\boldsymbol{\zeta}_j = \varphi(\boldsymbol{x}_j, t_j; t_{j+1}) - \boldsymbol{x}_{j+1}, \qquad j = 1, \ldots, N-1, \tag{20}$$

to vanish. Let the NLP variable vector be defined as

$$\boldsymbol{y} = \{\boldsymbol{x}_1, \boldsymbol{x}_2, \ldots, \boldsymbol{x}_N, t_1, t_N\}, \tag{21}$$

where the initial, final time, t_1, t_N, are let to vary, to allow the optimizer to converge to an optimal initial configuration and transfer duration. Let $\boldsymbol{\psi}_1 = \boldsymbol{\psi}_i(\boldsymbol{x}_1)$ and $\boldsymbol{\psi}_N = \boldsymbol{\psi}_f(\boldsymbol{x}_N)$. Then the vector of nonlinear equality constraints is given by

$$\boldsymbol{c}(\boldsymbol{y}) = \{\boldsymbol{\psi}_1, \boldsymbol{\zeta}_1, \boldsymbol{\zeta}_2, \ldots, \boldsymbol{\zeta}_{N-1}, \boldsymbol{\psi}_N\}. \tag{22}$$

The trajectory optimization has to avoid solutions which impact either the Earth or the Moon. This is imposed at each mesh point through

$$\begin{aligned}&(R_e/DU)^2-(x_j+\mu)^2+y_j^2<0,\\&(R_m/DU)^2-(x_j+\mu-1)^2+y_j^2<0,\quad j=1,\ldots,N.\end{aligned}\tag{23}$$

Moreover, the transfer duration has to be strictly positive; i.e. $t_1-t_N<0$. Thus, the vector of nonlinear inequality constraints is

$$\boldsymbol{g}(\boldsymbol{y})=\{\boldsymbol{\eta}_1,\boldsymbol{\eta}_2,\ldots,\boldsymbol{\eta}_N,\tau\},\tag{24}$$

where $\boldsymbol{\eta}_j=\boldsymbol{\eta}(\boldsymbol{x}_j)$ is the two-dimensional vector valued function defined by the left-hand sides of Eqs. (23) and $\tau=t_1-t_N$. The scalar objective function is

$$f(\boldsymbol{y})=\Delta v_1+\Delta v_N,\tag{25}$$

where $\Delta v_1=\Delta v_i(\boldsymbol{x}_1)$ and $\Delta v_N=\Delta v_f(\boldsymbol{x}_N)$, defined in Eq. (13) and (16), respectively. It is easy to verify that $\boldsymbol{y}$ is $(4N+2)$-dimensional, $\boldsymbol{c}$ is $4N$-dimensional, and $\boldsymbol{g}$ is $(2N+1)$-dimensional; with inequality constraints satisfied, the problem has $4N+2$ variables and $4N$ constraints.

NLP problem *Optimal, two-impulse Earth–Moon transfers are found by solving the NLP problem:*

$$\begin{aligned}\min_{\boldsymbol{y}}\ f(\boldsymbol{y})\ \text{subject to}\quad &\boldsymbol{c}(\boldsymbol{y})=\boldsymbol{0},\\&g_j(\boldsymbol{y})<0,\quad j=1,\ldots,2N+1.\end{aligned}\tag{26}$$

3.4 Continuation of optimal solutions

Once an optimal solution is found, it would be desirable to continue it in order to reconstruct, locally, the whole solution space. This is crucial to derive the totality of solutions and to characterize them. To do that, it is convenient to use the transfer duration as continuation parameter.

Suppose an optimal solution to problem (26) has been found: $\boldsymbol{y}=\{\boldsymbol{x}_1,\ldots,\boldsymbol{x}_N,t_1,t_N\}$. This solution has transfer duration $\Delta t=t_N-t_1$. The aim is to use $\boldsymbol{y}$ to derive a new optimal solution having a *fixed* duration $\Delta t'=\Delta t+\delta t$, where δt has to be small enough to allow the convergence to a new optimal solution. Thus, the new problem has to enforce the constraint on the transfer duration. This is done through the new condition

$$\sigma=t_N-t_1-\Delta t'=0,\tag{27}$$

that yields the augmented, $(4N+1)$-dimensional vector of equality constraints

$$\boldsymbol{c}'(\boldsymbol{y})=\{\boldsymbol{\psi}_1,\boldsymbol{\zeta}_1,\boldsymbol{\zeta}_2,\ldots,\boldsymbol{\zeta}_{N-1},\boldsymbol{\psi}_N,\sigma\}.\tag{28}$$

Continuation problem *Optimal solutions are continued in transfer duration by solving the NLP problem:*

$$\begin{aligned}\min_{\boldsymbol{y}}\ f(\boldsymbol{y})\ \textit{subject to}\quad &\boldsymbol{c}'(\boldsymbol{y})=\boldsymbol{0},\\&g_j(\boldsymbol{y})<0,\quad j=1,\ldots,2N+1.\end{aligned}\tag{29}$$

3.5 Implementation and verification

The optimization of two-impulse Earth–Moon transfers described above has been implemented within a numerical framework. The initial value problems (e.g., $\varphi(\boldsymbol{x}_j, t_j; t_{j+1})$) are solved with a variable-order, multi-step Adams–Bashforth–Moulton scheme (Shampine and Gordon 1975) with absolute and relative tolerances set to 10^{-14}. This stringent tolerance is imposed to have accurate solutions within the $N-1$ intervals in which the solution is split (when the $N-1$ pieces are put together, the solution has to be still accurate — provided that the equality constraints are satisfied with equally accurate tolerance).

The first guess solutions have been generated with the algorithm sketched in Sect. 3.2. The four-dimensional search space has been sampled with $I_\alpha = 361$, $J_\beta = 101$, $K_{t_i} = 13$, and $L_\delta = 101$. Thus, about 4.7×10^7 first guess orbits $\boldsymbol{\gamma}^{(ijkl)}$ have been generated.

The NLP problems (26) and (29) have been solved with a sequential quadratic programming algorithm implementing an active-set strategy (Gill et al. 1981) with tolerance on equality and inequality constraints of 10^{-10}. The gradient of the objective function (25) as well as the Jacobians of the equality and inequality constraints [Eqs. (22), (24), (28)] are calculated using a second-order central difference approximation. Once a solution to problem (26) is obtained, the entire family is computed by continuation [problem (29)] with values of δt of about $5 \times 10^{-2} TU$. In Fig. 5 the convergence history of a sample solution is reported. It can be seen that, although the final position of the initial guess misses the Moon by more than one Earth–Moon distance, the algorithm is still able to converge to an optimal solution.

Optimal solutions are verified a posteriori. If the solution is deemed sufficiently accurate, it is stored, otherwise it is discarded. The check is made by numerically integrating the optimal initial condition within the optimal time interval; i.e.

$$\overline{\boldsymbol{x}}_f = \varphi(\boldsymbol{x}_1, t_1; t_N). \tag{30}$$

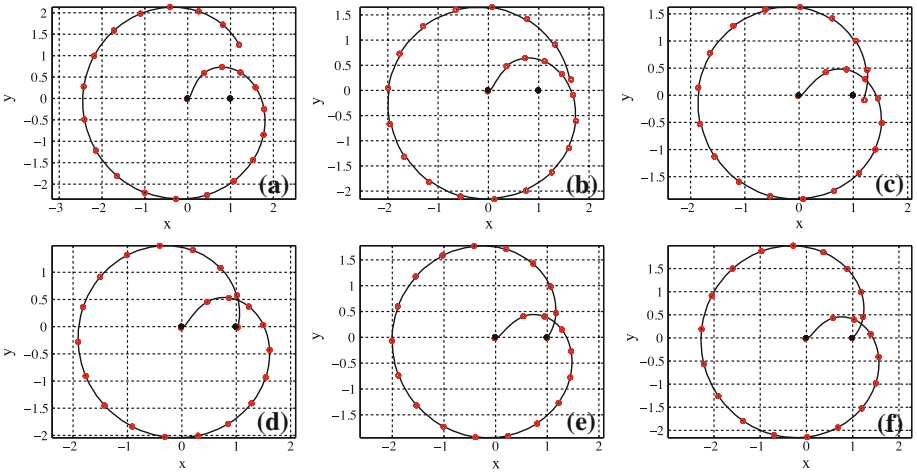

Fig. 5 Iterative solutions of the NLP problem (26). Each figure reports the iteration and the maximum equality constraint violation (max c_j). The first guess (Iter 0) is in Fig. 5a. This is generated with $\alpha = 1.5\pi$, $\beta = 1.41$, $t_i = 0$, $\delta = 7$ (see Sect. 3.2). This solution has $N = 23$ mesh points (red bullets in the figures); this yields 94 variables and 92 equality constraints. Convergence has been achieved in 29 iterations. **a** Iter 0; max $c_j = 1.866$; **b** Iter 3; max $c_j = 0.475$; **c** Iter 6; max $c_j = 0.203$; **d** Iter 10; max $c_j = 0.078$; **e** Iter 20; max $c_j = 0.397$; **f** Iter 29; max $c_j = 3.9\text{e-}11$

The final state $\overline{\boldsymbol{x}}_f$ has to be as close as possible to the optimal final state $\boldsymbol{x}_f$. For a solution to be accepted it is required that $\max\{|\boldsymbol{\psi}_1(\boldsymbol{x}_1)|, |\boldsymbol{\psi}_N(\overline{\boldsymbol{x}}_f)|\} \leq 10^{-8}$; i.e. the *real* trajectory violates the boundary conditions by less than 10^{-8} scaled units ($\sim$3 m in length and $\sim$ 0.01 m/s in speed). Moreover, it is also checked that the real optimal solution impacts neither the Earth nor the Moon. As the impact-free constraint is imposed only on the mesh points through Eqs. (23), the verification is done from end to end, by re-integrating the solution starting from the optimal initial condition; i.e.

$$\eta_j(\boldsymbol{x}(t)) < 0, \quad t \in [t_1,\ t_N], \quad j = 1, 2, \tag{31}$$

with $\boldsymbol{x}(t) = \varphi(\boldsymbol{x}_1, t_1; t)$, and $\boldsymbol{\eta}(\boldsymbol{x})$ as from Sect. 3.3, Eqs. (23).

4 Optimal solutions

4.1 The global picture

The optimal solutions found are reported in Fig. 6. Each point of the figure is associated to an optimal solution with duration Δt and cost Δv (these two quantities are re-scaled using the time and speed units in Table 3). In total, approximately 5×10^5 optimal solutions have been found, many of which are not displayed in Fig. 6 (having $\Delta v > 4150$ m/s or $\Delta t > 100$ days). Figure 6 suggests that the solutions are organized into families, and these families constitute a well-defined structure in the $(\Delta t,\ \Delta v)$ plane, thus confirming the conjecture in Sect. 1.4. The families have been achieved by continuation with the procedure shown in Sect. 3.4. This procedure generates also spurious points not belonging to any known structure. These are the points in which continuation of solutions fails, and are not considered in the analysis below.

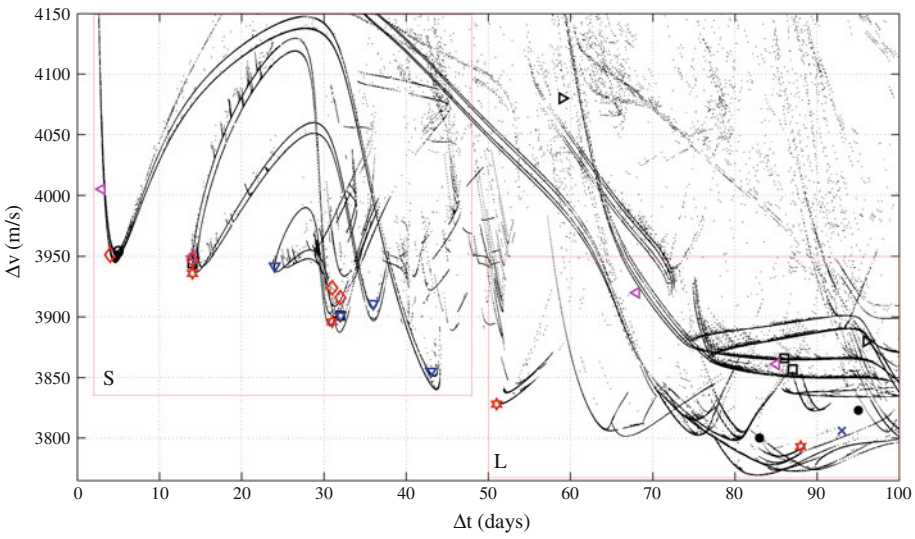

Fig. 6 Optimal two-impulse Earth–Moon transfers, shown in the $(\Delta t, \Delta v)$ plane. The two regions S and L enclose "Short" and "Long" transfer solutions, respectively. The reference solutions in Fig. 1 are superimposed (legend in Fig. 1)

It is noted that the existence of optimal solutions is not guaranteed for every combination of $(\Delta t,\ \Delta v)$. This explains the existence of empty areas between families.

A question arises: how do these optimal solutions relate to those found in previous studies? To answer this question, the reference solutions in Fig. 1 are superimposed on the points of Fig. 6. A good matching is found between the solutions found and those taken from the literature. In particular, the reference solutions appear to be sample points of the reconstructed solutions set, and, most importantly, almost all of them are located in the regions about the local minima of the function $\Delta v(\Delta t)$.

For fixed transfer time, the solutions having a lower cost are of more interest in the investigation below. To ease the analysis, the total set of solutions in Fig. 6 is subdivided into two regions that enclose "Short" and "Long"transfers ('S' and 'L' squares in Fig. 6, respectively). Considering one region at a time helps characterizing the families of solutions, and allows us to better focus on the solutions deemed of interest. This is done in Sect. 5.

4.2 Pareto-efficient solutions

Although Fig. 6 is generated within a simplified, planar gravitational model, the total solutions set may serve to mission designers as a catalogue: first guess values for duration and cost can be extracted for preliminary estimations, and the corresponding solutions may be refined in more complete models. In this perspective, it would be desirable to extract those solutions for which the balance between Δt and Δv is optimal. In the framework of multi-objective optimization, this means computing the Pareto front of solutions, made up by the *nondominated* points.

Definition 2 (*Pareto optimality*) Let $\boldsymbol{y}_i$ and $\boldsymbol{y}_j$ be two solutions of Problem (26) (or Problem (29)) defined as in (21); let $\Delta v(\boldsymbol{y}) = f(\boldsymbol{y})$ in (25) and let $\Delta t(\boldsymbol{y}) = t_N - t_1$. The solution $\boldsymbol{y}_i$ strictly dominates $\boldsymbol{y}_j$, or $\boldsymbol{y}_i \succ \boldsymbol{y}_j$, if the following conditions are both satisfied:

(i) $\Delta t(\boldsymbol{y}_i) \leq \Delta t(\boldsymbol{y}_j)$ and $\Delta v(\boldsymbol{y}_i) \leq \Delta v(\boldsymbol{y}_j)$,
(ii) $\Delta t(\boldsymbol{y}_i) < \Delta t(\boldsymbol{y}_j)$ or $\Delta v(\boldsymbol{y}_i) < \Delta v(\boldsymbol{y}_j)$.

The Pareto front is the set of points that are not strictly dominated by another point.

In Fig. 7, the Pareto front for the set of solutions in Fig. 6 is reported. In practice, the points belonging to the Pareto front correspond to the solutions having the best balance between cost and time. This is worthwhile for real Earth–Moon transfers, provided that the mission constraints do not prevent the choice of a solution belonging to the Pareto front. As a matter of example, the coordinates of the ten sample Pareto-efficient solutions shown in Fig. 7 are reported in Table 4. Moving from left to right, the solutions range from the Hohmann-like transfer (i) to a particular exterior low energy transfer (x), which is the cheapest solution found in the entire work ($\Delta v = 3769.3$ m/s). The transfers corresponding to the points in Fig. 7, except for solution (vii) whose shape is similar to that of (viii), are reported in Fig. 8 in the Earth-centered, inertial frame. The conversion to the Earth-centered inertial frame is given in Appendix 1. *The initial condition,* $\boldsymbol{x}_i = (x_i, y_i, \dot{x}_i, \dot{y}_i)$, *and the initial, final time,* t_i, t_f, *for each of these ten solutions, are reported in Table A of the supplement appended to the online version of the article.*

4.3 Angular momentum at final time

The problem statement and, more specifically, the final boundary conditions (14)–(15), enforce the final transfer state, $\boldsymbol{x}_f = (x_f, y_f, \dot{x}_f, \dot{y}_f)$, to be at a physical distance r_f from

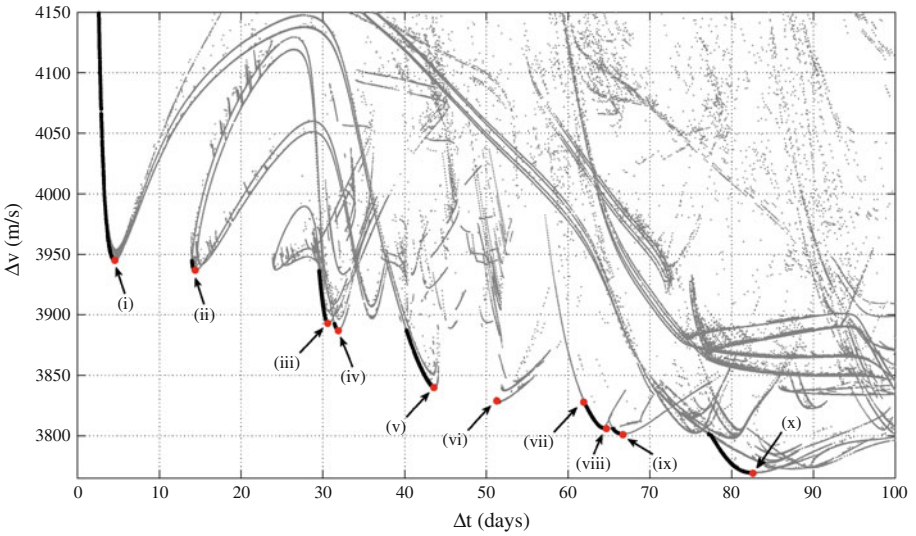

Fig. 7 Pareto front (*black*) associated to the global set of optimal solutions (*grey*). The coordinates of the ten sample Pareto-efficient points (*red dots*) are reported in Table 4

Table 4 Example of Pareto-efficient solutions in Fig. 7; Δt in days, Δv in m/s

Point	(i)	(ii)	(iii)	(iv)	(v)	(vi)	(vii)	(viii)	(ix)	(x)
Δt	4.6	14.4	30.6	31.9	43.6	51.3	61.9	64.6	66.7	82.6
Δv	3944.8	3936.6	3892.7	3887.4	3840.0	3828.6	3828.9	3805.9	3801.4	3769.3

The initial condition and initial, final time for each of these solutions are reported in Table A (supplement to the online article)

the Moon and to have the velocity parallel to the local circular velocity. Yet, these conditions do not specify the direction of the final velocity, so allowing the possibility of having both *direct* and *retrograde* final orbits around the Moon. These are discriminated by computing the angular momentum with respect to the Moon associated to $\boldsymbol{x}_f$, $h_{2,f} = h_2(\boldsymbol{x}_f)$, through Eq. (10). Direct orbits are those orbits for which $h_{2,f} > 0$; retrograde orbits have instead $h_{2,f} < 0$. The sign of $h_{2,f}$ for the total solution set in Fig. 6 is highlighted in Fig. 9.

It can be noticed that, for fixed transfer time, solutions belonging to the same family have different costs according to the sign of $h_{2,f}$. Moreover, there is no apparent way to establish a priori whether the direct or retrograde final orbits are more convenient without having fixed the transfer time. For instance, by considering the local minima in Fig. 9(left), we can infer that acquiring a direct final orbit around the Moon is more convenient for $\Delta t \lesssim 25$ days; retrograde final orbits become more convenient in the range $25 \lesssim \Delta t \lesssim 72$ days (see also Fig. 9(right)). For $72 \lesssim \Delta t \lesssim 90$ days the Δv of direct final orbits is lower than that of retrograde orbits, and this conditions is again reversed for $90 \lesssim \Delta t \lesssim 100$ days. In summary, the analysis of the final angular momentum at the Moon shows that the total set of solutions is organized into a nontrivial structure, which can be understood by a thorough characterization of the families.

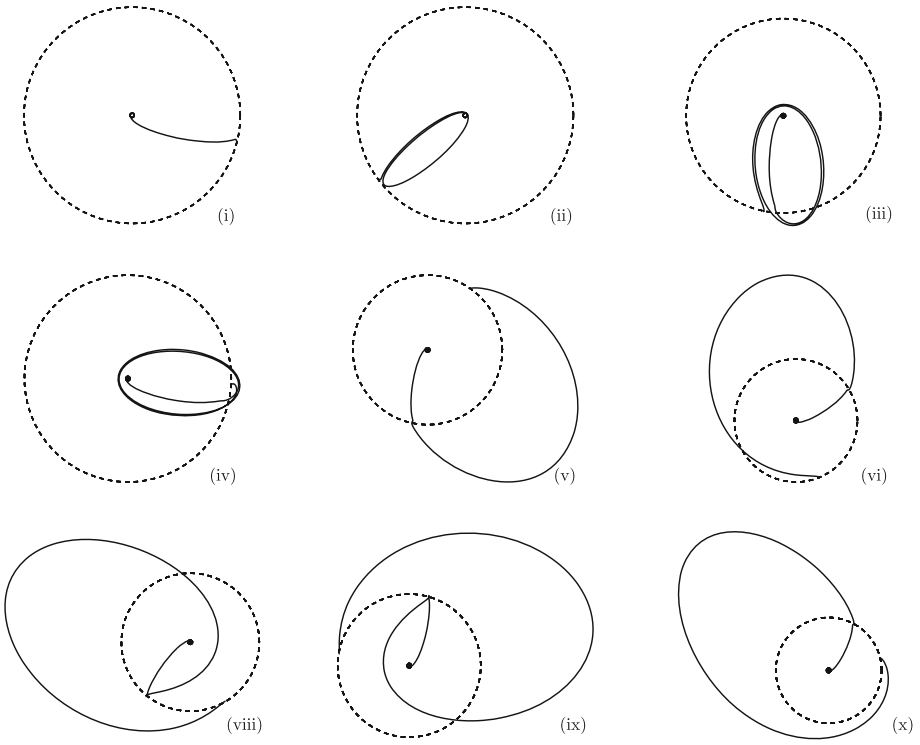

Fig. 8 The Pareto-efficient Earth–Moon transfers indicated in Fig. 7 shown in the Earth-centered inertial frame (the Moon orbit is *dashed*). Solution (vii) is very similar to solution (viii) and therefore it is not shown

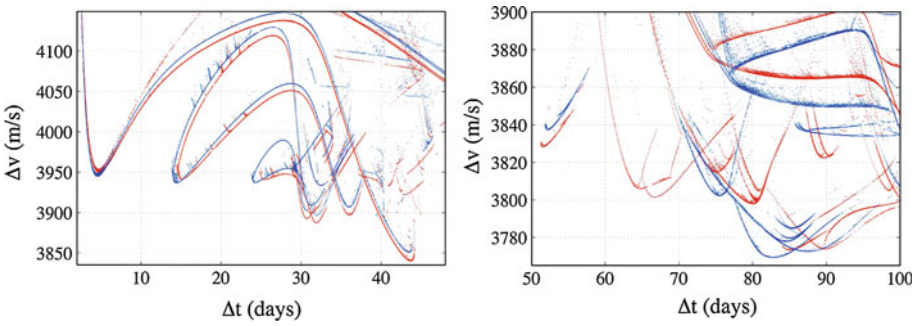

Fig. 9 Angular momentum with respect to the Moon at the final time, $h_{2,f}$, in the $(\Delta t,\ \Delta v)$ plane. Direct (*blue*) and retrograde (*red*) final orbits around the Moon. (*left*) S region; (*right*) L region

4.4 Kepler energy at final time

The spacecraft may (or may not) experience ballistic capture upon Moon arrival. To detect those solutions that exhibit ballistic capture it is sufficient to compute the Kepler energy with respect to the Moon at the final time, $H_{2,f} = H_2(\boldsymbol{x}_f)$, through Eqs. (8)–(9). If $H_{2,f} < 0$, then P is temporary ballistically captured by the Moon according to Definition 1 (it is straightforward that the Kepler energy with respect to the Moon is positive at departure). If $H_{2,f} > 0$, there is no ballistic capture at arrival.

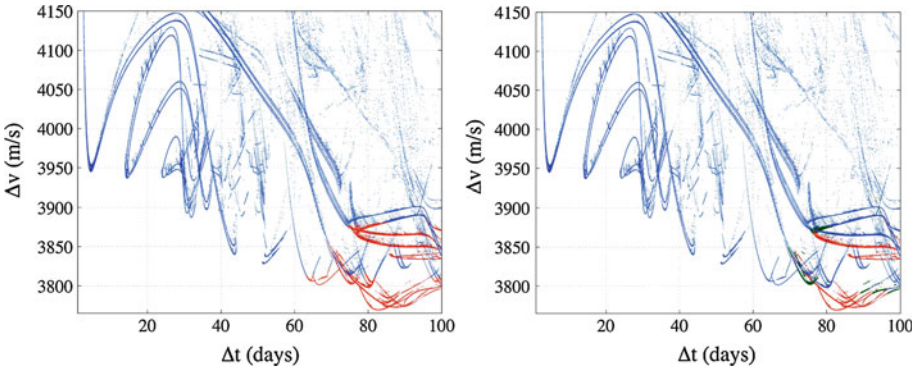

Fig. 10 Kepler and Jacobi energies at the final time. (*left*) Kepler energy at final time, $H_{2,f} < 0$ red, $H_{2,f} > 0$ blue; (*right*) Jacobi energy at final time, case b) *red*, c) *green*, d) *blue*

In Fig. 10(left) the sign of $H_{2,f}$ is highlighted for the total set of solutions in Fig. 6 (ballistic captured solutions are reported in red). It can be noticed that only a subset of the total solution set performs lunar ballistic capture at arrival. These are those cases located in the bottom-right part of the $(\Delta t, \Delta v)$ plane; i.e. the solutions with long transfer time and low cost. With reference to Fig. 8, only solutions (8), (9), and (10) are ballistically captured at the Moon. While solution (10) belongs to the well-known class of exterior low energy transfers (Belbruno and Miller 1993; Belbruno 2004; Parker et al. 2011; Parker and Anderson 2011; Yamakawa et al. 1992, 1993), the other two [solutions (8) and (9)] deserve further analysis.

4.5 Jacobi energy at final time

In the PBRFBP, in which the optimal two-impulse Earth–Moon transfers are achieved, the Jacobi energy is no longer an integral of motion. However, computing the Jacobi energy at the final time, $J_f = J(\boldsymbol{x}_f)$ via Eq. (3), helps understanding the geometry of Hill's regions upon Moon arrival, where the perturbation of the Sun can be neglected. Moreover, J_f is an indicator of the energy level of interior transfers, where the Sun perturbation has little influence (Yagasaki 2004a,b; Mengali and Quarta 2005). In addition, the exterior low energy transfers can be formulated with the patched restricted three-body problem approximation, which fixes the Jacobi energy in the Earth–Moon system (Koon et al. 2001; Parker 2006; Parker and Lo 2006; Mingotti and Topputo 2011; Mingotti et al. 2011b, 2012).

The value of J_f for the total solution set in Fig. 6 has been calculated through Eq. (3), and the four energy ranges mentioned in Sect. 2.1 (Fig. 2) have been highlighted in Fig. 10(right). First of all, it can be noticed that no solutions belonging to case a) are found. This is due to the fact that, in the PCRTBP, orbits defined at energies $C_2 < J < C_1$, do not approach low altitude Earth orbits (Bolt and Meiss 1995; Schroer and Ott 1997; Macau 2000; Ross 2003). For the Earth–Moon transfer to occur at this energy level, a multi-impulse strategy has to be considered (Pernicka et al. 1995; Topputo et al. 2005a). Transfers belonging to case b) are shown red in Fig. 10(right). These are associated to the bottom-right part of the $(\Delta t, \Delta v)$ plane, where low energy transfers exist. Thus, with the patched restricted three-body problems approximation, where energies $C_3 < J < C_2$ are required, a subset of the ballistic captured solutions ($H_{2,f} < 0$, Fig. 10) can be obtained. Case c) (green points in Fig. 10(right)) is associated to solution not belonging to the Pareto front (Fig. 7); these transfers are characterized in Sect. 5. Finally, case d) (blue points in Fig. 10(right)) encloses

the vast majority of solutions found. This means that the interior and a portion of the exterior transfers have final energies that allow P to move in the entire physical space; thus, P can approach the Moon from any direction. By comparing Figs. 7 and 10(right), it can be observed that solutions (vii)–(ix) belong to case d); i.e. solutions of this kind cannot be found with the patched restricted three-body problems approximation.

5 Characterization of transfers

In this section the optimal two-impulse Earth–Moon solutions are characterized. Given the global set in Fig. 6, only those solutions showing the best balance in terms of cost and transfer time are considered for brevity's sake. In Fig. 6 many of the computed optimal two-impulse transfers are observed to construct some sets of similar curves. Using this structure, we classify the optimal transfers into some families below.

The solutions are parameterized by using the four scalars $\{\alpha, \beta, t_i, \delta\}$. In Sect. 3.2 these numbers are used to define a first guess solution. In this section they are extrapolated a posteriori from the optimal solution at hand. This is done to present the optimal solutions in a concise form, using parameters having geometrical or physical meaning. (Alternatively, $\boldsymbol{x}_1, t_1, t_N$ could have been given, but this involves reporting six numbers – instead of four – with no direct meaning). These four numbers are given with high accuracy (12 decimals) for some sample solutions in each family. This allows an independent reproduction of the optimal solutions through the approach sketched in Sect. 3.2.

Let $\boldsymbol{x}_1 = (x_1, y_1, \dot{x}_1, \dot{y}_1)$, t_1, t_N be the optimal initial condition and the initial, final time, respectively. The angle that locates the initial point on the Earth parking orbit is

$$\alpha = \arctan\left(\frac{y_1}{x_1 + \mu}\right), \tag{32}$$

whereas the initial-to-circular velocity ratio is

$$\beta = \sqrt{\frac{r_0}{1-\mu}}\left(r_0 + \sqrt{\dot{x}_1^2 + \dot{y}_1^2}\right). \tag{33}$$

For the analysis below it is convenient to keep track of the initial phase of the Sun (in place of the initial time t_i). This is given by $\theta_i = \omega_s t_1$, modulo 2π. The last parameter is simply $\delta = t_N - t_1$.

A thorough investigation has been conducted to analyze the optimal solutions. In particular, for each solution the following quantities have been tracked (beside $\{\alpha, \beta, \theta_i, \delta\}$): angular momentum and Kepler energy with respect to the Moon at final time ($h_{2,f}$ and $H_{2,f}$), Jacobi energy at final time (J_f), magnitude of the second impulse (Δv_f), and total cost (Δv). These quantities are reported in dimensionless units except for Δv and Δv_f which are given in m/s. Dimensional values can be achieved through the units in Table 3. Solutions giving rise to similar transfers that differ only by the sign of $h_{2,f}$ are deemed to belong to the same family. Direct and retrograde final orbits are discriminated by using the superscript '+' and '−', and called 'positive' and 'negative', respectively (see Sect. 4.3). For each family both positive and negative solutions are shown, provided that both of them exist. Some figures are reported in Appendix 2 for brevity. It is worth pointing out that only those families deemed of interest have been characterized. Many other solutions exist, which are not shown below.

The tables reporting the solutions data (Tables B–J) are published as supplementary material and are appended to the online version of the paper.

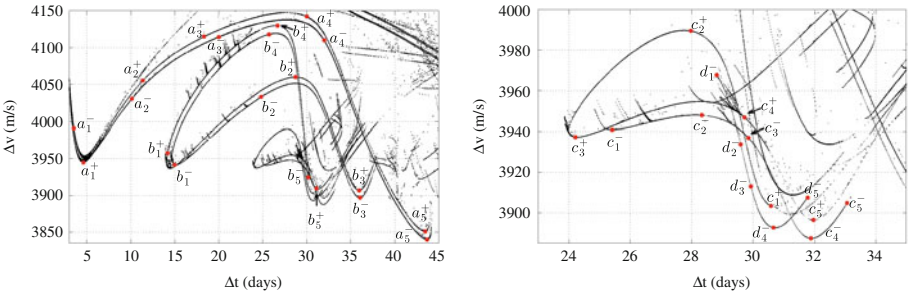

Fig. 11 Families a, b, c, d in the $\Delta t, \Delta v$ plane. (*left*) Families a, b; (*right*) Families c, d

5.1 The S region

The S region contains solutions whose transfer time is less than 50 days (see Fig. 6). The dynamics of the solutions lying in this region are mostly governed by the Earth and Moon gravitation attractions. For this reason, each of the sample solutions reported is shown in both the Earth–Moon rotating frame and the Earth-centered, inertial frame. In the latter reference system, it is useful to define n_r as the number of revolutions of P (the spacecraft) around P_1 (the Earth).

5.1.1 Family a

Family a is made up of transfers with $n_r = 0$; i.e. Earth–Moon transfers that do not perform a complete revolution around the Earth. In the $(\Delta t, \Delta v)$ plane, family a has two local minima, located at $\Delta t \simeq 5$ days, $\Delta t \simeq 44$ days, respectively (Fig. 11(left)). Ten sample solutions are reported in Table B (five positive, five negative). The solution a_1^+ corresponds to a Hohmann-like transfer with prograde final orbit around the Moon ($\Delta t = 4.59$ days, $\Delta v = 3944.8$ m/s). When moving along the family for increasing Δt, the transfers approach the Moon in no favorable conditions, and this explains the local maximum at about $\Delta t \simeq 27$ days. Then, the cost of the solutions decreases due to the presence of lunar close encounters (see Figs. 12 and 24(left)). This gives rise to the minimum represented by solutions a_5^+ and a_5^-. These solutions cost up to 105 m/s less than the Hohmann transfer with a transfer time of approximately 44 days. Some examples in Yagasaki (2004a,b); Mengali and Quarta (2005) fall into family a (see Fig. 6).

5.1.2 Family b

Family b is formed by transfers with $n_r = 1$; i.e. orbits that perform one complete revolution around the Earth. For each of the two branches (positive and negative) family b shows three local minima and two local maxima in the $(\Delta t, \Delta v)$ plane (see Fig. 11(left)). The three minima are represented by the solutions $b_1^\pm, b_3^\pm, b_5^\pm$, whose parameters are reported in Table C. The first minimum ($b_1^\pm$) corresponds to solutions having the same cost of the Hohmann transfer but Δt three times higher. Again, when moving from this minimum toward increasing Δt, the cost increases accordingly until lunar close encounters appear and the two local minima arise. The geometry of these solutions can be seen in Figs. 13 and 24(right). Reference solutions belonging to family b can be found in Yagasaki (2004a,b); Mengali and Quarta (2005); Mingotti and Topputo (2011); see Fig. 6.

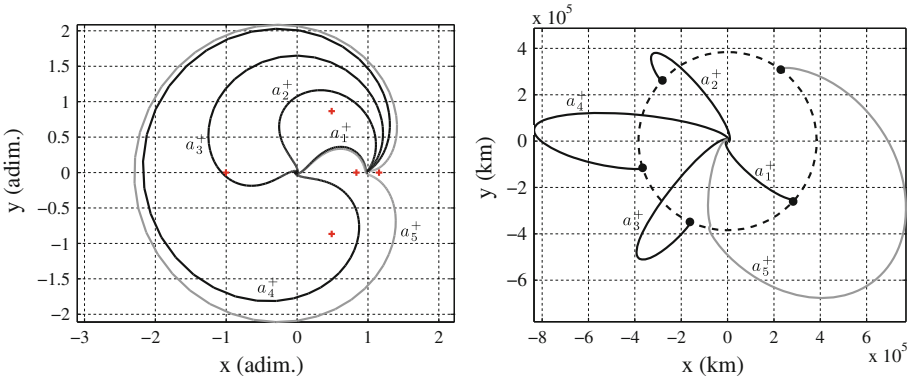

Fig. 12 Positive solution samples belonging to family a. Different scales of grey are used from now on to ease the understanding of the figures. (*left*) Rotating frame; (*right*) Earth-centered inertial frame

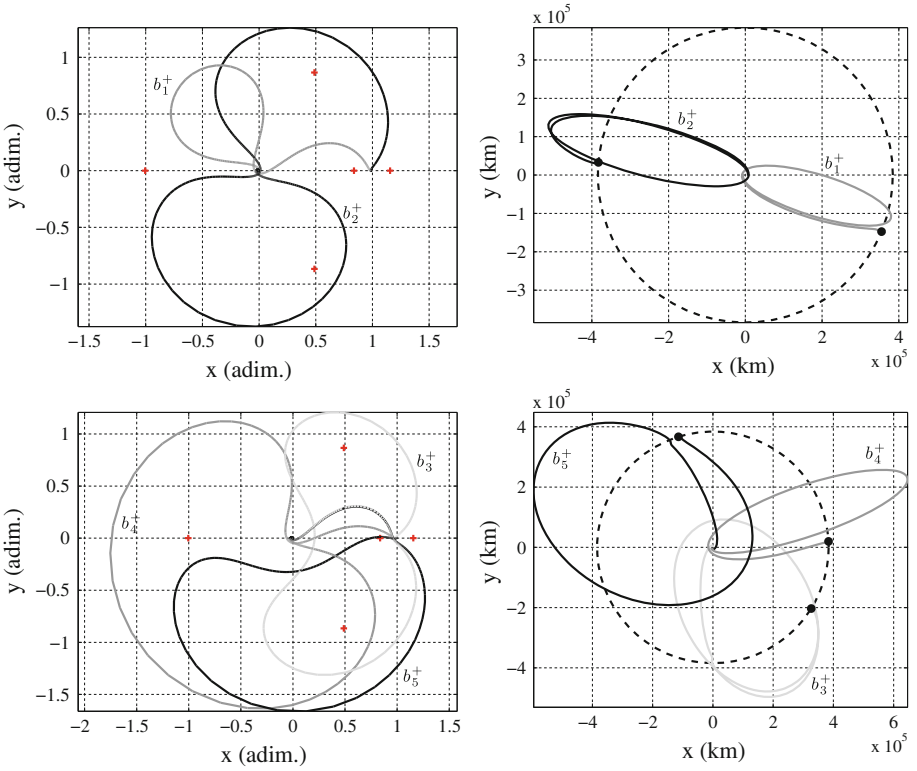

Fig. 13 Positive solution samples belonging to family b. (*left*) Rotating frame; (*right*) Earth-centered inertial frame

5.1.3 Families c, d

In families c, d the particle P performs two revolutions around the Earth, and thus $n_r = 2$. These two families are defined in the range $\Delta t \simeq 24$–34 days (see Fig. 11(right)). No positive family d is found. Family c has two local minima (at $\Delta t \simeq 24$ and 32 days) and two local

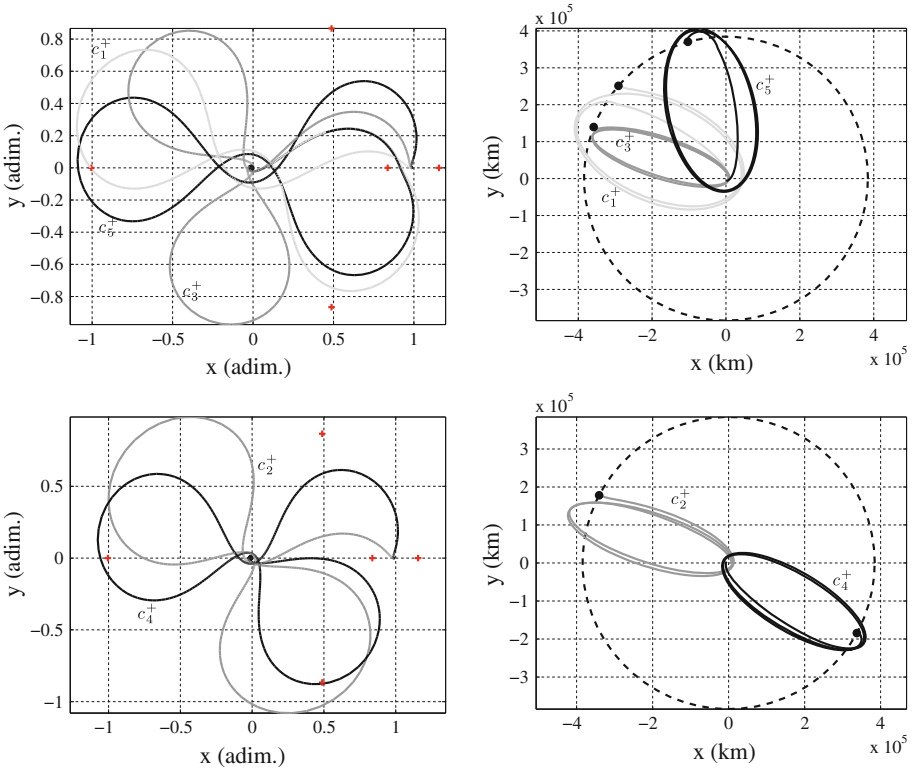

Fig. 14 Positive solution samples belonging to family c. (*left*) Rotating frame; (*right*) Earth-centered inertial frame

maxima (both at $\Delta t \simeq 28$ days). Family d has a local minimum at $\Delta t \simeq 31$. The parameters of families c, d are reported in Table D and the corresponding trajectories are shown in Figs. 14 and 25. The trajectories in family d are very similar to those of family c, and thus they are not reported. The examples in Yagasaki (2004a,b); Mingotti and Topputo (2011) can be deemed belonging to family c, d; see Fig. 6. All of the solutions shown so far may be classified within the class of interior transfers. Solutions similar to those of families a^+, b^+, and c^+ have been found in Yagasaki (2004a,b). The families a^-, b^-, c^-, and d^- presented in this paper further enrich the set of two-impulse Earth–Moon interior transfers.

5.2 The L region

The L region encloses solutions with transfer time longer than 50 days (and shorter than 100 days; see Fig. 6). The dynamics that governs this subset of solutions is characterized by the Sun perturbation, as the corresponding trajectories spend most of the transfer time well outside the Moon orbit (Fig. 8). For this reason, the sample solutions analyzed below are shown in both the Earth-centered and the Sun–Earth rotating frame. The latter is a co-rotating system of reference centered at the Sun–Earth barycenter where the Sun and the Earth are at rest. In this frame the Sun–Earth equilibrium points, $L_{1,SE}$ and $L_{2,SE}$, are shown as well. In normalized Sun–Earth units, these two points are located at $x_{L_{1,SE}} = 0.9900266828$ and $x_{L_{2,SE}} = 1.0100340264$, and their energy is $C_{1,SE} = 3.0003004051$ and $C_{2,SE} =$

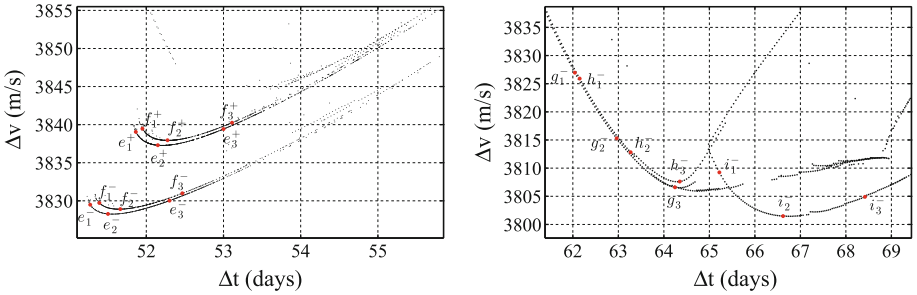

Fig. 15 Families e, f, g, h, i in the Δt, Δv plane. (*left*) Families e, f; (*right*) Families g, h, i

3.0003000446, respectively. These values are obtained with the Sun–Earth mass parameter $\mu_{SE} = 3.0034 \times 10^{-6}$ (Szebehely 1967). The trajectory visualization in the Sun–Earth rotating frame is done to both catch the dynamics governing the L-region transfers and check which quadrant the solutions belong to (see Sect. 1.1).

Beside the orbit of the Moon, the plots in the Earth-centered inertial frame report the counterclockwise apparent orbit of the Sun (dashed, not to scale; the initial and final positions of the Sun are labelled with bullets). In the Earth-centered inertial frame of Figs. 16, 17, 19, 20, 22, 23, two dash-dot lines are also drawn: these connect the Earth with both the farthest point of the trajectory (Earth–apogee line) and the Sun location when P is at apogee (Earth–Sun line). The role played by the angle formed by these two lines in the exterior transfers dynamics is discussed in Circi and Teofilatto (2001). As many families characterize the L region, three solutions are reported for each family, and the trajectory of one sample solution per family is illustrated for brevity's sake.

5.2.1 Families e, f

With reference to Fig. 15(left), families e, f are defined in the range $\Delta t \simeq 50$ to 55 days. This is one of the few cases in which there is a remarkable difference in cost between positive and negative transfers, the latter being about 10 m/s (minimum-to-minimum) more convenient than the former. From a geometrical point of view, families e, f give rise to short-lasting exterior transfers performing lunar gravity assist. Family e is made up of second quadrant solutions (Fig. 16), while family f contains fourth quadrant transfers (Fig. 26(top-left)). Unlike the families belonging to the S region, these solutions can be achieved only within narrow ranges of the initial angular position of the Sun (see Table E), indicating the importance of its perturbation. The peculiarity of these two families is that the Moon is approached from the interior although most of the trajectory is defined outside the Moon orbit. No ballistic capture is performed at arrival ($H_{2,f} > 0$ in Table E), and the final Jacobi energy (J_f in Table E) indicates that there are no forbidden regions at arrival. In the literature, a solution close to e_2^- has been found in Mingotti and Topputo (2011); see Fig. 6.

5.2.2 Families g, h, i

These three families exist in the range $\Delta t \simeq 60$ to 72 days, where they form two minima (at $\Delta t \simeq 64$ and 67 days, respectively; see Fig. 15(right)). Only positive g and negative h, i solutions are found (Table F). These solutions show unique features: the transfer orbit foresees a lunar gravity assist that places P in a close Earth encounter orbit, followed by an

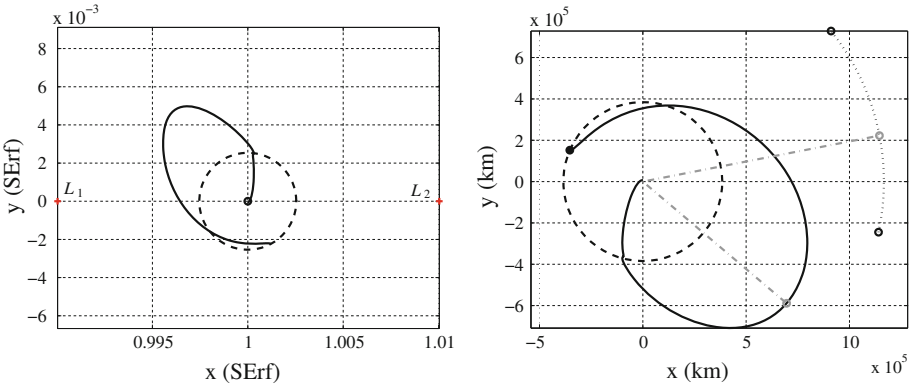

Fig. 16 Solution e_2^- belonging to family e. (*left*) Sun–Earth rotating frame; (*right*) Earth-centered inertial frame

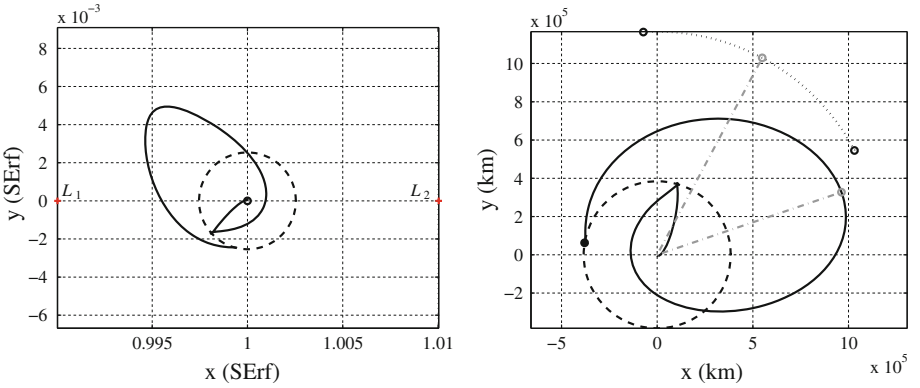

Fig. 17 Solution i_2^- belonging to family i. (*left*) Sun–Earth rotating frame; (*right*) Earth-centered inertial frame

exterior-like transfer (see Figs. 17 and 26(top-right)). Families g, i generate second quadrant transfers, whereas family h contains fourth quadrant solutions. The function $H_{2,f}$ changes sign along these families, and therefore ballistic capture appears according to Definition 1. This occurs even though $J_f < 3$, which means that there are no forbidden regions for P upon Moon arrival. With reference to Fig. 6, no reference solutions having these features are found in the literature (to the best of the author's knowledge).

5.2.3 Families j, k

Families j, k are defined within $\Delta t \simeq 72$ and 82 days (see Fig. 18(left)). These present two minima at $\Delta t \simeq 75$ and 80, respectively. Positive j and negative k solutions are found. Together with families g, h, i, these solutions show a transition between ballistic capture and escape upon Moon arrival (see the sign of $H_{2,f}$ in Table G). However, these solutions have $J_f \cong 3$, meaning that the energy level at Moon arrival is close to $C_{4,5}$. Families j, k are made up by second, fourth quadrant transfers, respectively. The geometry of the trajectories recalls that of an exterior transfer with lunar gravity assist, although from the Sun–Earth rotating frames it can be inferred that the dynamics of $L_{1,SE}$ and $L_{2,SE}$ is not exploited (i.e.

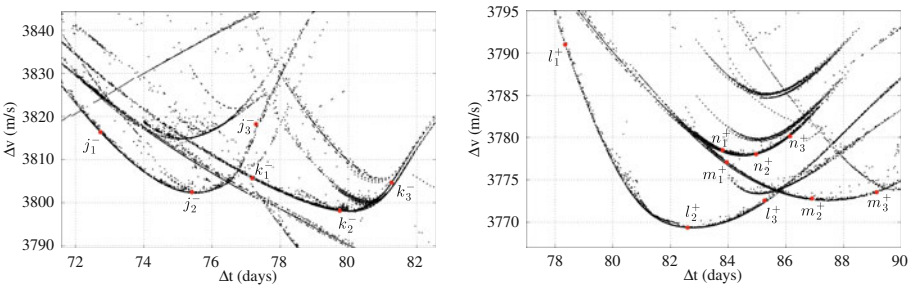

Fig. 18 Families j, k, l, m, n in the Δt, Δv plane. (*left*) Families j, k; (*right*) Families l, m, n

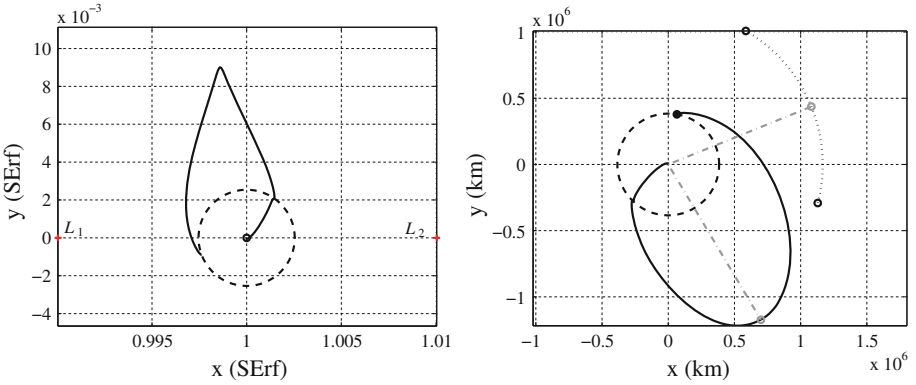

Fig. 19 Solution j_2^+ belonging to family j. (*left*) Sun–Earth rotating frame; (*right*) Earth-centered inertial frame

the trajectories are neither close to possible $L_{1/2,SE}$ periodic orbit nor their manifolds; see Fig. 19). No reference solutions are found in the region families j, k belong to (Fig. 6).

5.2.4 Families l, m, n

These three families are defined within $\Delta t \simeq 78$ and 90 days. Each of the three families presents a local minimum, with the one of family l being the global minimum of the whole $\Delta v(\Delta t)$ function (see Fig. 18(right)). This is located at $\Delta t = 82.6$ days, $\Delta v = 3769.3$ m/s. From the solution parameters summarized in Table H it can be inferred that: 1) only positive transfers are found; 2) all of the solutions perform ballistic capture at Moon arrival ($H_{2,f} < 0$); 3) the final value of the Jacobi energy at arrival satisfies $C_3 \leq J_f < C_2$ (see Table 2). The latter condition corresponds to the case b) discussed in Sect. 2.1 and is shown in Figs. 2 and 10(right). From Figs. 20 (solution l_2^+, the global minimum) and 26(center-left) (solution m_2^+) it can be seen that all of the transfers are second quadrant solutions performing a lunar gravity assist. In particular, it can be seen that the post-swing-by orbit in m_2^+ is in 3:1 resonance with the Moon orbit. It is important to notice that these transfers (the best in terms of total cost) do not exploit the $L_{1/2,SE}$ invariant manifolds structure. Reference solutions matching any of these three families are not found, though examples in Yamakawa et al. (1992, 1993); Mingotti and Topputo (2011) are defined in the same region of families l, m, n (Fig. 6).

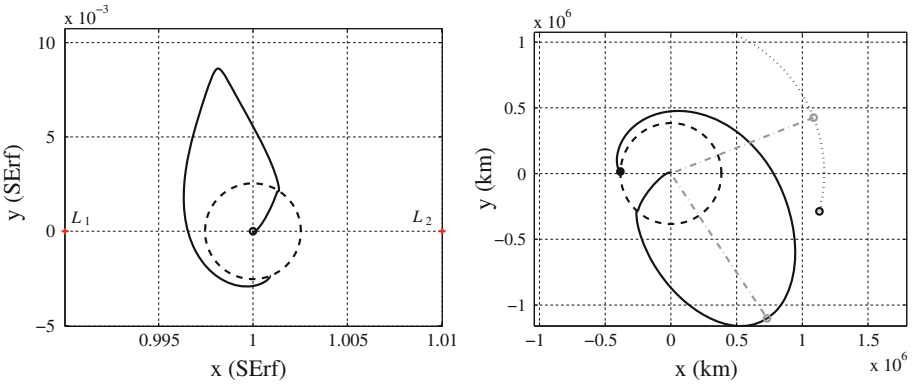

Fig. 20 Solution l_2^+ belonging to family l. (*left*) Sun–Earth rotating frame; (*right*) Earth-centered inertial frame

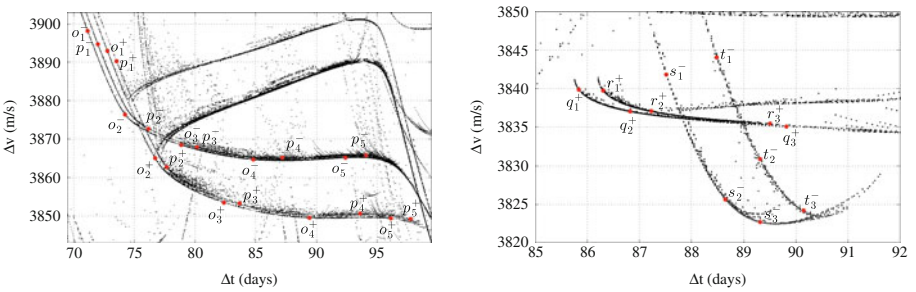

Fig. 21 Families o, p, q, r, s, t in the Δt, Δv plane. (*left*) Families o, p; (*right*) Families q, r, s, t

5.2.5 *Families o, p*

Families o, p span a wide range of transfer times, from $\Delta t \simeq 70$ to 100 days, with a transfer cost that drops 50 m/s along the families. Both positive and negative solutions are found for the two families, the former being cheaper than the latter for $\Delta t > 75$ (see Fig. 21(left)). The dynamics of these solutions recall that of a classic exterior transfer (see Fig. 22, solution o_5^+, second quadrant transfer, and Fig. 26(center-right), solution p_5^-, fourth quadrant transfer). No lunar gravity assist exists, and this explains the variability of α in Table I (departure may occur in any direction, if the Moon has not to be encountered, provided that a suitable value of θ_i is considered). From Table I, a direct relation between transfer cost and final Kepler energy at Moon arrival can be observed. When $H_{2,f}$ decreases, Δv decreases accordingly. These families are close to the reference solutions in Mengali and Quarta (2005); Da Silva Fernandes and Marinho (2011); Assadian and Pourtakdoust (2010) and adhere to the trajectories used in GRAIL mission (Hoffman 2009; Roncoli and Fujii 2010; Chung et al. 2010; Hatch et al. 2010); see Fig. 6.

5.2.6 *Families q, r, s, t*

The branches defining these families are reported in Fig. 21(right) and their parameters are summarized in Table J. Solutions s, t perform a lunar gravity assist similar to families g, h, i,

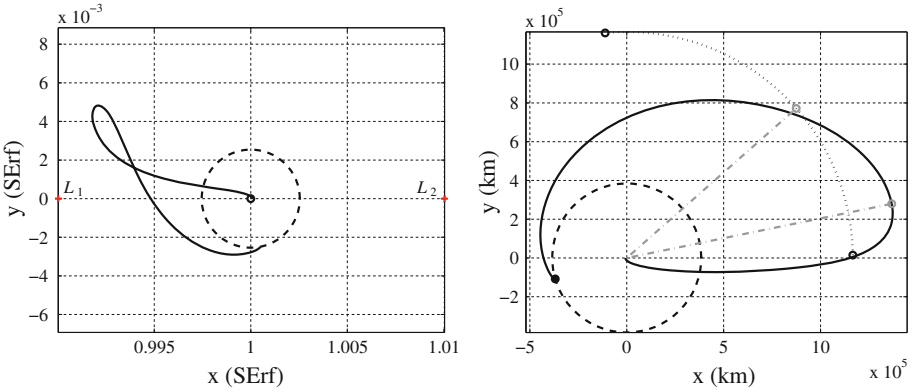

Fig. 22 Solution o_5^+ belonging to family o. (*left*) Sun–Earth rotating frame; (*right*) Earth-centered inertial frame

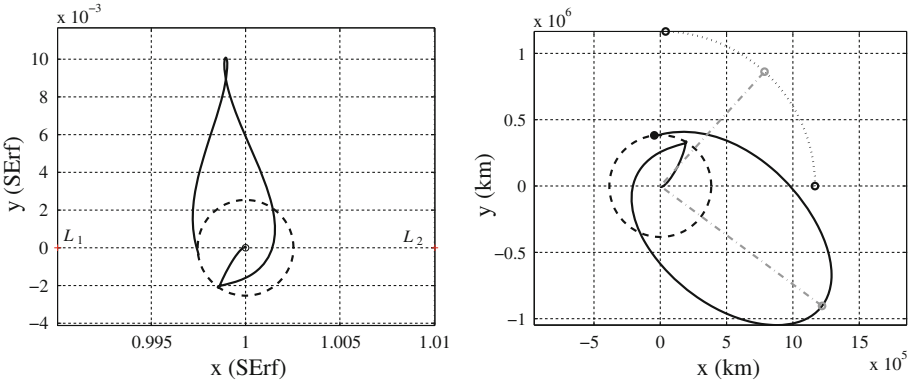

Fig. 23 Solution s_3^- belonging to family s. (*left*) Sun–Earth rotating frame; (*right*) Earth-centered inertial frame

although no ballistic capture is accomplished (see Fig. 23, solution s_3^-, second quadrant transfer). Families q, r exploit instead the dynamics of the Sun–Earth Lagrange points and their transfer structure recalls that of families o, p (see Fig. 26(bottom row), solution q_2^+, second quadrant transfer). With reference to Fig. 6, no reference solutions close to these families are found.

6 Conclusions

Since the discovery of low-energy transfers, the problem of finding alternative, efficient Earth–Moon transfers has been approached with a focus on a small class of solutions, if not on just *one* kind of solutions. Typically, when a novel solution is found, one compares it to the Hohmann transfer, leaving unanswered the question on the existence of other solutions, possibly having intermediate features between the solution at hand and the Hohmann transfer. This modus operandi prevents the formulation of a complete trade-off between cost and transfer time.

Motivated by this need, the present paper reconstructs the global set of solutions for the two-impulse Earth–Moon transfers. The idea is to view the Hohmann, the interior, and the exterior transfers as special solutions of the same problem. This means that known cases may be thought of as belonging to a more general picture. The framework used in this paper is the $(\Delta t, \Delta v)$ plane, which allows direct assessment of solutions for practical purposes.

The global set of optimal two-impulse Earth–Moon transfers presented in this paper demonstrates that the intuition on the existence of intermediate solutions was valid. Known solutions reduce to points belonging to different families of transfers. The families deemed of more interest have been characterized and studied in detail, and their main features have been discussed. The parameters defining all the solutions presented are given to allow the reproduction of these transfers for possible further independent investigations.

Acknowledgments The author is grateful to Pierluigi Di Lizia, Alexander Wittig, and Koen Geurts for having proof-read the paper, to Mauro Massari and Franco Bernelli-Zazzera for having shared their workstations, and to Roberto Armellin for the computation of the Pareto-efficient solutions.

Appendix 1

An orbit in the rotating frame, $\boldsymbol{x}(t) = \{x(t), y(t), \dot{x}(t), \dot{y}(t)\}$, is converted to an orbit expressed in the P_1-centered (or Earth-centered), inertial frame, $\boldsymbol{X}_1(t) = \{X_1(t), Y_1(t), \dot{X}_1(t), \dot{Y}_1(t)\}$, through

$$\begin{aligned} X_1(t) &= (x(t) + \mu)\cos t - y(t)\sin t \\ Y_1(t) &= (x(t) + \mu)\sin t + y(t)\cos t \\ \dot{X}_1(t) &= (\dot{x}(t) - y(t))\cos t - (\dot{y}(t) + x(t) + \mu)\sin t \\ \dot{Y}_1(t) &= (\dot{x}(t) - y(t))\sin t + (\dot{y}(t) + x(t) + \mu)\cos t \end{aligned} \tag{34}$$

where t is the present, scaled time. The transformation into the P_2-centered (i.e. Moon-centered), inertial frame is obtained from (34) by replacing 'μ' with '$\mu - 1$'.

Appendix 2

The figures corresponding to the solutions characterized in Sect. 5 are reported below (see Figs. 24, 25, 26).

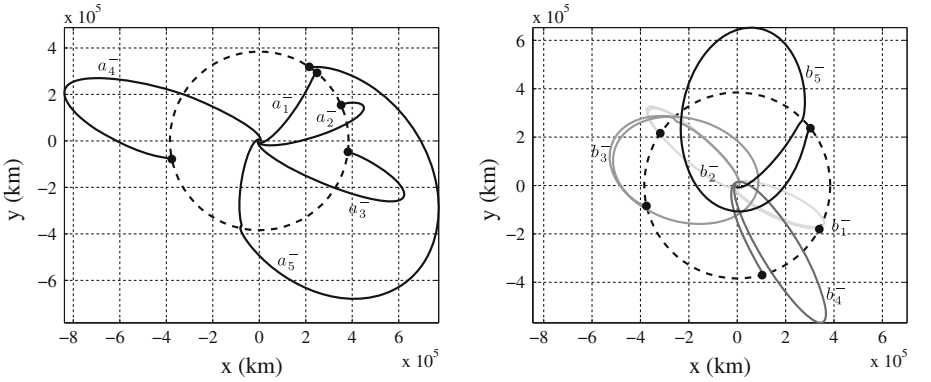

Fig. 24 Negative solution samples belonging to family a and b in the Earth-centered inertial frame. (*left*) Family a^-; (*right*) Family b^-

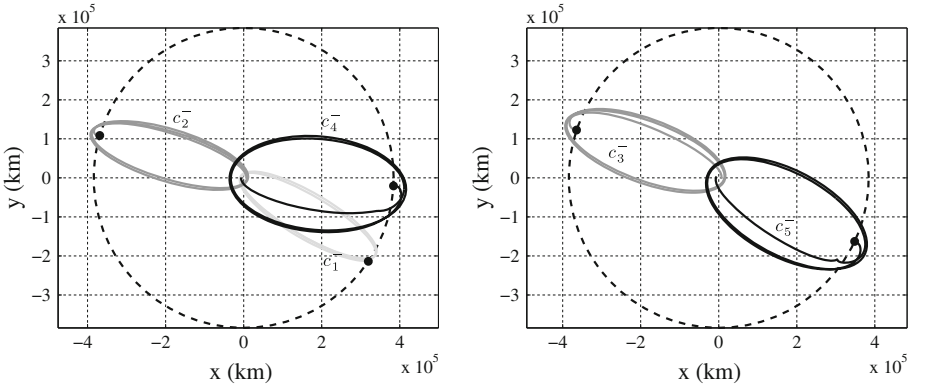

Fig. 25 Negative solution samples belonging to family c in the Earth-centered inertial frame. (*left*) Solutions c_1^-, c_2^-, c_4^-; (*right*) c_3^-, c_5^-

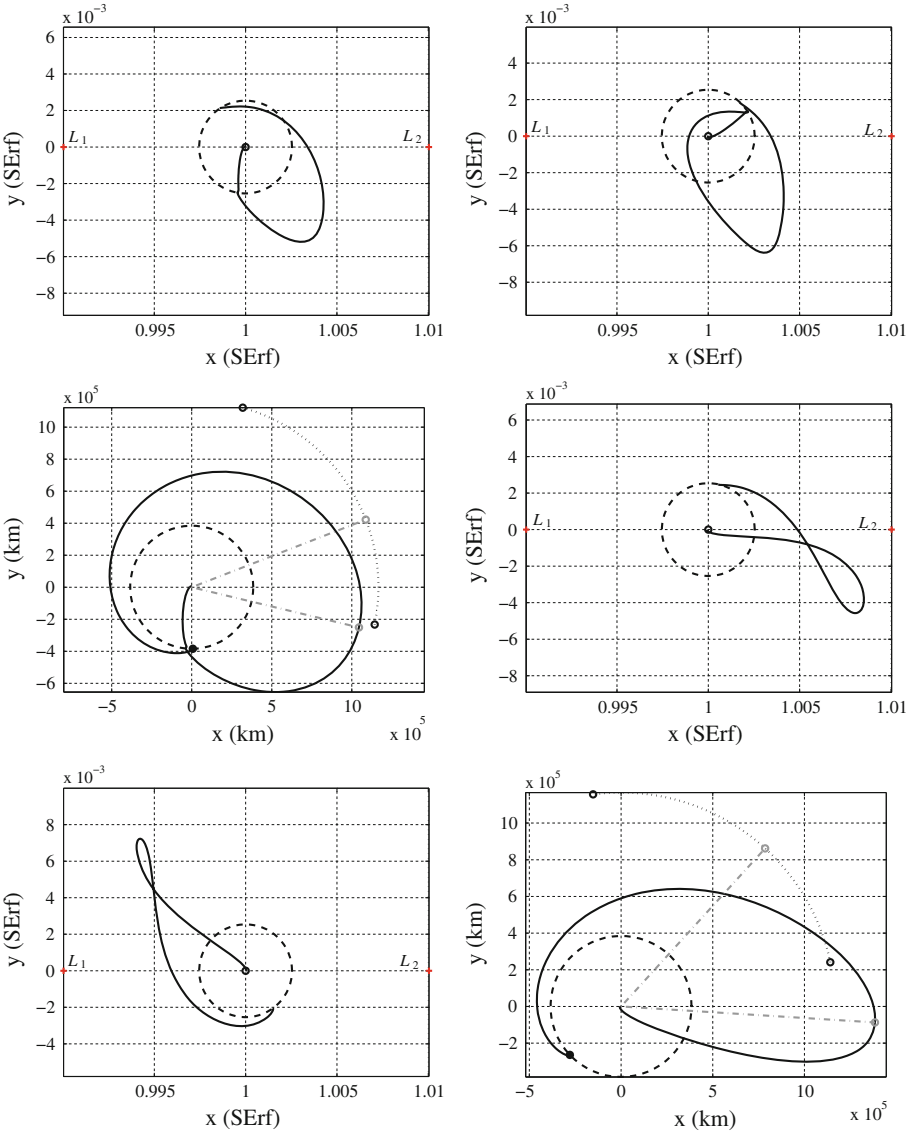

Fig. 26 Sample solutions (*top-left*) f_1^+; (*top-right*) h_3^-; (*center-left*) m_2^+; (*center-right*) p_5^-; (*bottom row*) q_2^+

References

Armellin, R., Di Lizia, P., Topputo, F., Lavagna, M., Bernelli-Zazzera, F., Berz, M.: Gravity assist space pruning based on differential algebra. Celest. Mech. Dyn. Astron. **106**(1), 1–24 (2010). doi:10.1007/s10569-009-9235-0

Assadian, N., Pourtakdoust, S.H.: Multiobjective genetic optimization of Earth–Moon trajectories in the restricted four-body problem. Adv. Space Res. **45**(3), 398–409 (2010)

Battin, R.H.: An Introduction to the Mathematics and Methods of Astrodynamics. AIAA, New York (1987)

Belbruno, E.: Lunar capture orbits, a method of constructing Earth–Moon trajectories and the lunar GAS mission. In: AIAA Paper 97–1054, Proceedings of the AIAA/DGLR/JSASS International Electric Propulsion Conference (1987)
Belbruno, E.: The dynamical mechanism of ballistic lunar capture transfers in the four-body problem from the perspective of invariant manifolds and Hill's regions. In: Technical Report, Centre de Recerca Matematica, Barcelona, Spain (1994)
Belbruno, E.: Capture Dynamics and Chaotic Motions in Celestial Mechanics: With Applications to the Construction of Low Energy Transfers. Princeton University Press, Princeton (2004)
Belbruno, E., Carrico, J.: Calculation of weak stability boundary ballistic lunar transfer trajectories. In: AIAA/AAS Astrodynamics Specialist Conference, Paper AIAA 2000–4142 (2000)
Belbruno, E., Miller, J.: Sun-perturbed Earth-to-Moon transfers with ballistic capture. J. Guid. Control Dyn. **16**, 770–775 (1993)
Belbruno, E., Gidea, M., Topputo, F.: Weak stability boundary and invariant manifolds. SIAM J. Appl. Dyn. Syst. **9**(3), 1061–1089 (2010)
Belbruno, E., Topputo, F., Gidea, M.: Resonance transition associated to weak capture in the restricted three-body problem. Adv. Space Res. **42**(8), 18–39 (2008). doi:10.1016/j.asr.2008.01.018
Belló-Mora, M., Graziani, F., Teofilatto, P., Circi, C., Porfilio, M., Hechler, M.: A systematic analysis on weak stability boundary transfers to the Moon. In: Paper iaf-00-a.6.03, Proceedings of the 51st International Astronautical Conference (2000)
Betts, J.T.: Survey of numerical methods for trajectory optimization. J. Guid. Control Dyn. **21**, 193–207 (1998)
Biesbroek, R., Janin, G.: Ways to the Moon? ESA Bull. **103**, 92–99 (2000)
Bolt, E.M., Meiss, J.D.: Targeting chaotic orbits to the Moon through recurrence. Phys. Lett. A **204**, 373–378 (1995)
Castelli, R.: Nonlinear Dynamics of Complex Systems: Applications in Physical, Biological and Financial Systems. Springer, New York (2011)
Chung, M.J., Hatch, S.J., Kangas, J.A., Long, S.M., Roncoli, R.B., Sweetser, T.H.: Trans-lunar cruise trajectory design of GRAIL (gravity recovery and interior laboratory) mission. In: Paper AIAA 2010–8384, AIAA Guidance, Navigation, and Control Conference, Toronto, Ontario, Canada, 2–5 August (2010)
Circi, C.: Properties of transit trajectory in the restricted three and four-body problem. Adv. Space Res. **49**, 1506–1519 (2012)
Circi, C., Teofilatto, P.: On the dynamics of weak stability boundary lunar transfers. Celest. Mech. Dyn. Astron. **79**(1), 41–72 (2001)
Circi, C., Teofilatto, P.: Weak stability boundary trajectories for the deployment of lunar spacecraft constellations. Celest. Mech. Dyn. Astron. **95**(1), 371–390 (2006)
Conley, C.C.: Low energy transit orbits in the restricted three-body problem. SIAM J. Appl. Math. **16**, 732–746 (1968)
Da Silva Fernandes, S., Marinho, C.M.P.: Sun influence on two-impulsive Earth-to-Moon transfers. In: Proceedings of the 22nd International Symposium on Space Flight Dynamics, Sao José dos Campos, Brazil, 28 Feb–4 March (2011)
De Melo, C.F., Winter, O.C.: Alternative paths to Earth–Moon transfer. Math. Probl. Eng. **2006**, 1–20 (2006)
Enright, P.J., Conway, B.A.: Discrete approximations to optimal trajectories using direct transcription and nonlinear programming. J. Guid. Control Dyn. **15**, 994–1002 (1992)
Gill, P.E., Murray, W., Wright, M.H.: Practical Optimization. Academic, London (1981)
Gómez, G., Koon, W.S., Lo, M.W., Marsden, J.E., Masdemont, J., Ross, S.D.: Invariant manifolds, the spatial three-body problem and space mission design. Adv. Astronaut. Sci. **109**(1), 3–22 (2001)
Hatch, S.J., Roncoli, R.B., Sweetser, T.H.: Trans-lunar cruise trajectory design of GRAIL (Gravity Recovery and Interior Laboratory) Mission. In: Paper AIAA 2010–8385, AIAA Guidance, Navigation, and Control Conference, Toronto, Ontario, Canada, 2–5 august, (2010).
Hoffman, T. L.: GRAIL: gravity mapping the Moon. In: IEEE Aerospace Conference, Big Sky, Montana, USA, 7–14 March 2009, 1–8. IEEE (2009)
Hyeraci, N., Topputo, F.: Method to design ballistic capture in the elliptic restricted three-body problem. J. Guid. Control Dyn. **33**(6), 1814–1823 (2010)
Hyeraci, N., Topputo, F.: The role of true anomaly in ballistic capture. Celest. Mech. Dyn. Astron. **116**(2), 175–193 (2013)
Ivashkin, V.V.: On trajectories of Earth–Moon flight of a particle with its temporary capture by the Moon. Dokl. Phys. **47**(11), 196–199 (2002)
Koon, W.S., Lo, M.W., Marsden, J.E., Ross, S.D.: Shoot the Moon. In: AAS/AIAA Astrodynamics Specialist Conference, Paper AAS 00–166 (2000)
Koon, W.S., Lo, M.W., Marsden, J.E., Ross, S.D.: Low energy transfer to the Moon. Celest. Mech. Dyn. Astron. **81**, 63–73 (2001)

Macau, E.E.N.: Using chaos to guide a spacecraft to the Moon. Acta Astronaut. **47**, 871–878 (2000)
Mengali, G., Quarta, A.: Optimization of biimpulsive trajectories in the Earth–Moon restricted three-body system. J. Guid. Control Dyn. **28**, 209–216 (2005)
Miele, A., Mancuso, S.: Optimal trajectories for Earth–Moon–Earth flight. Acta Astronaut. **49**(2), 59–71 (2001)
Mingotti, G., Topputo, F.: Ways to the Moon: a survey. In: Paper AAS 11–283, 21th AAS/AIAA Space Flight Mechanics Meeting, New Orleans, USA, 13–17 February (2011)
Mingotti, G., Topputo, F., Bernelli-Zazzera, F.: Low-energy, low-thrust transfers to the Moon. Celest. Mech. Dyn. Astron. **105**(1–3), 61–74 (2009a). doi:10.1007/s10569-009-9220-7
Mingotti, G., Topputo, F., Bernelli-Zazzera, F.: Numerical methods to design low-energy, low-thrust Sun-perturbed transfers to the Moon. In: Proceedings of the 49th Israel Annual Conference on Aerospace Sciences, Tel Aviv, Haifa, Israel (2009b)
Mingotti, G., Topputo, F., Bernelli-Zazzera, F.: Earth–Mars transfers with ballistic escape and low-thrust capture. Celest. Mech. Dyn. Astron. **110**(2), 169–188 (2011a). doi:10.1007/s10569-011-9343-5
Mingotti, G., Topputo, F., Bernelli-Zazzera, F.: Optimal low-thrust invariant manifold trajectories via attainable sets. J. Guid. Control Dyn. **34**(6), 1644–1656 (2011b). doi:10.1007/s10569-011-9343-5
Mingotti, G., Topputo, F., Bernelli-Zazzera, F.: Efficient invariant-manifold, low-thrust planar trajectories to the Moon. Commun. Nonlinear Sci. Numer. Simul. **17**(2), 817–831 (2012). doi:10.1016/j.cnsns.2011.06.033
Parker, J.S.: Families of low-energy lunar halo transfers. In: Paper AAS 06–132, AAS/AIAA Spaceflight Mechanics Conference, Tampa, FL, USA, 22–26 Jan (2006)
Parker, J.S., Anderson, R.L.: Targeting low-energy transfers to low lunar orbit. In: AIAA/AAS Astrodynamics Specialist Conference, Girdwood, Alaska, USA, 31 July–4 August (2011)
Parker, J.S., Lo, M.W.: Shoot the Moon 3D. Adv. Astronaut. Sci. **123**, 2067–2086 (2006)
Parker, J.S., Anderson, R.L., Peterson, A.: A survey of ballistic transfers to low lunar orbit. In: Advances in the Astronautical Sciences, Proceedings of the 21st AAS/AIAA Space Flight Mechanics Meeting, New Orleans, USA, 13–17 Feb, 2011, vol. 140, pp. 2481–2500. Univelt, Inc. (2011)
Peng, L., Wang, Y., Dai, G., Chang, Y., Chen, F.: Optimization of the Earth–Moon low energy transfer with differential evolution based on uniform design. In: IEEE Congress on Evolutionary Computation, Barcelona, Spain, 18–23 July, 2010, 1–8. IEEE (2010). doi:10.1109/CEC.2010.5586384
Pernicka, H.J., Scarberry, D.P., Marsh, S.M., Sweetser, T.H.: A search for low Δv Earth-to-Moon trajectories. J. Astronaut. Sci. **43**, 77–88 (1995)
Perozzi, E., Di Salvo, A.: Novel spaceways for reaching the Moon: an assessment for exploration. Celest. Mech. Dyn. Astron. **102**(1), 207–218 (2008)
Roncoli, R.B., Fujii, K.K.: Mission design overview for the gravity recovery and interior laboratory (GRAIL) mission. In: Paper AIAA 2010–8383, AIAA Guidance, Navigation, and Control Conference, Toronto, Ontario, Canada, 2–5 August (2010)
Ross, S.D.: Trade-off between fuel and time optimization. In: Proceeding of the New Trends in Astrodynamics and Applications (2003)
Schoenmaekers, J., Horas, D., Pulido, J.A.: SMART-1: with solar electric propulsion to the Moon. In: Proceeding of the 16th International Symposium on Space Flight, Dynamics (2001)
Schroer, C.G., Ott, E.: Targeting in hamiltonian systems that have mixed regular/chaotic phase spaces. Chaos **7**, 512–519 (1997)
Shampine, L.F., Gordon, M.K.: Computer Solution of Ordinary Differential Equations: The Initial Value Problem. W.H. Freeman, San Francisco (1975)
Simó, C., Gómez, G., Jorba, Á., Masdemont, J.: The Bicircular Model Near the Triangular Libration Points of the RTBP. From Newton to Chaos. Plenum Press, New York (1995)
Sweetser, T.H.: An estimate of the global minimum Δv needed for Earth–Moon transfer. Adv. Astronaut. Sci. **75**, 111–120 (1991)
Szebehely, V.: Theory of Orbits: The Restricted Problem of Three Bodies. Academic, San Diego (1967)
Topputo, F., Belbruno, E.: Computation of weak stability boundaries: Sun–Jupiter system. Celest. Mech. Dyn. Astron. **105**(1–3), 3–17 (2009). doi:10.1007/s10569-009-9222-5
Topputo, F., Belbruno, E., Gidea, M.: Resonant motion, ballistic escape, and their applications in astrodynamics. Adv. Space Res. **42**(8), 6–17 (2008). doi:10.1016/j.asr.2008.01.017
Topputo, F., Vasile, M., Bernelli-Zazzera, F.: Earth-to-Moon low energy transfers targeting L_1 hyperbolic transit orbits. Ann. N.Y. Acad. Sci. **1065**, 55–76 (2005a)
Topputo, F., Vasile, M., Bernelli-Zazzera, F.: Low energy interplanetary transfers exploiting invariant manifolds of the restricted three-body problem. J. Astronaut. Sci. **53**(4), 353–372 (2005b)
Winter, O.C., Vieira Neto, E., Prado, A.F.B.A.: Orbital maneuvers using gravitational capture times. Adv. Space Res. **31**(8), 2005–2010 (2003)

Yagasaki, K.: Computation of low energy Earth-to-Moon transfers with moderate flight time. Physica D **197**(3–4), 313–331 (2004a)

Yagasaki, K.: Sun-perturbed Earth-to-Moon transfers with low energy and moderate flight time. Celest. Mech. Dyn. Astron. **90**, 197–212 (2004b)

Yamakawa, H., Kawaguchi, J., Ishii, N., Matsuo, H.: A numerical study of gravitational capture orbit in the Earth–Moon system. In: Spaceflight Mechanics 1992; Proceedings of the 2nd AAS/AIAA Meeting, Colorado Springs, CO, Feb 24–26, pp. 1113–1132 (1992)

Yamakawa, H., Kawaguchi, J., Ishii, N., Matsuo, H.: On Earth–Moon transfer trajectory with gravitational capture. Adv. Astronaut. Sci. **85**, 397–397 (1993)